Mitochondrial dysfunction promotes aquaporin expression that controls hydrogen peroxide permeability and ferroptosis

Yuko Takashi[a,b,#], Kazuo Tomita[a,#], Yoshikazu Kuwahara[a,c], Mehryar Habibi Roudkenar[a,d], Amaneh Mohammadi Roushandeh[a,e], Kento Igarashi[a], Taisuke Nagasawa[a], Yoshihiro Nishitani[b], Tomoaki Sato[a,*].

[a]Departments of Applied Pharmacology and [b]Restorative Dentistry and Endodontology, Graduate School of Medical and Dental Sciences, Kagoshima University, Kagoshima, Japan

[c]Division of Radiation Biology and Medicine, Faculty of Medicine, Tohoku Medical and Pharmaceutical University, Sendai, Japan

[d]Cardiovascular Diseases Research Center, Department of Cardiology, Heshmat Hospital, School of Medicine, Guilan University of Medical Sciences, Rasht, Iran

[e]Medical Biotechnology Department, Paramedicine Faculty, Guilan University of Medical Sciences, Rasht, Iran

#: These two authors contributed equally to this work

*: Corresponding author: Tomoaki Sato, Department of Applied Pharmacology, Graduate School of Medical and Dental Sciences, Kagoshima University, Kagoshima, Japan. *Email address:* tomsato@dent.kagoshima-u.ac.jp

Abbreviations: AQP, aquaporin; DFO, deferoxamine; DFX, deferasirox; ETC, electron transport chain; H_2O_2, hydrogen peroxide; HeLa, Human cervical cancer; Mito cell, mitochondria transferred cells; mtDNA, mitochondrial DNA; NOX2, nicotinamide-adenine dinucleotide phosphate oxidase 2; PHB2, prohibitin2; Phe, phenanthroline; RPMI Roswell Park Memorial Institute; SAS, oral squamous cell carcinoma; WST, the water-soluble tetrazolium.

Abstract

Most anti-cancer agents and radiotherapy exert their therapeutic effects via the production of free radicals. Ferroptosis is a recently described cell death process that is accompanied by iron-dependent lipid peroxidation. Hydrogen peroxide (H_2O_2) has been reported to induce cell death. However, it remains controversial whether H_2O_2-induced cell death is ferroptosis. In the present study, we aimed to elucidate the involvement of mitochondria in H_2O_2-induced ferroptosis and examined the molecules that regulate ferroptosis. We found that one mechanism underlying H_2O_2-induced cell death is ferroptosis, which occurs soon after H_2O_2 treatment (within 3 h after H_2O_2 treatment). We also investigated the involvement of mitochondria in H_2O_2-induced ferroptosis using mitochondrial DNA-depleted ρ^0 cells because ρ^0 cells produce more lipid peroxidation, hydroxyl radicals ($^{\bullet}OH$), and are more sensitive to H_2O_2 treatment. We found that ρ^0 cells contain high Fe^{2+} levels that lead to $^{\bullet}OH$ production by H_2O_2. Further, we observed that aquaporin (AQP) 3, 5, and 8 bind nicotinamide-adenine dinucleotide phosphate oxidase 2 and regulate the permeability of extracellular H_2O_2, thereby contributing to ferroptosis. Additionally, the role of mitochondria in ferroptosis was investigated using mitochondrial transfer in ρ^0 cells. When mitochondria were transferred into ρ^0 cells, the cells exhibited no sensitivity to H_2O_2-induced cytotoxicity because of decreased Fe^{2+} levels. Moreover, mitochondrial transfer upregulated the mitochondrial quality control protein prohibitin 2 (PHB2), which contributes to reduced AQP expression. Our findings also revealed the involvement of AQP and PHB2 in ferroptosis. Our results indicate that H_2O_2 treatment enhances AQP expression, Fe^{2+} level, and lipid peroxidation, and decrease mitochondrial function by downregulating PHB2, and thus, is a promising modality for effective cancer treatment.

Keywords: mitochondria, ferroptosis, aquaporin, hydrogen peroxide, Fe^{2+}

Introduction

There are numerous chemotherapeutic agents that exert their effects via production of free radicals and/or reactive oxygen species (ROS) [1-5]. Among broad sense ROS, hydrogen peroxide (H_2O_2) is used as a sensitizer in cancer treatment during radiation therapy. H_2O_2 treatment resolves the hypoxic state in tumor tissue by downregulating internal peroxidase activity and enables the generation of superoxide ($O_2^{\bullet -}$) for radiation therapy [6, 7]. ROS are highly reactive and oxidize intracellular components such as DNA, proteins, and lipids, leading to cell death [8]. Intracellular ROS are generated by various enzymatic reactions such as nicotinamide-adenine dinucleotide phosphate oxidase (NOX) in the cytoplasm, but the mitochondrial electron transport chain (ETC) is thought to be the main source of intracellular ROS, especially hydroxyl radicals ($^{\bullet}OH$) [9, 10].

Mitochondria have their own DNA (mtDNA) that encodes 13 proteins, which are components of the ETC. Damage to mtDNA produces a higher amount of ROS that, in turn, plays an important role in cancer initiation, promotion, and chemo/radio resistance [11, 12]. We previously established mtDNA-depleted cells (ρ^0 cells) from two cancer cell lines, i.e. cervical cancer (HeLa) and oral squamous cell carcinoma (SAS). We observed that the ρ^0 cells exhibit sensitivity to ROS, particularly H_2O_2, because the ρ^0 cell plasma membrane includes more lipid peroxides than their parental cells. In short, the membrane lipid components were changed by the influence of H_2O_2, and H_2O_2 more easily permeates the plasma membrane. Indeed, liposome membrane experiments showed that increased lipid peroxidation content leads to more H_2O_2 permeation, at least up to 5-10% lipid peroxidation [13, 14]. Furthermore, the ρ^0 cells showed higher aquaporin (AQP) gene expression [15]. Importantly, AQPs are involved in the diffusion of H_2O_2 as well as H_2O [16-18].

Mitochondria are not only the main intracellular organelle of ROS production, but also the main metabolic site for iron regulation. The influx of cytoplasmic Fe^{2+} into mitochondria mainly uses a system of heme and iron-sulfur (Fe/S) clusters. Heme functions as an active center of hemoglobin, cytochrome p450, and cytochrome oxidase, while Fe/S clusters function in the ETC and in vitamin

synthesis [19, 20]. When Fe^{2+} is increased, $^{\bullet}OH$ is produced through the Fenton reaction in the presence of Fe^{2+} and H_2O_2. $^{\bullet}OH$ induces lipid peroxidation in the plasma membrane, which leads to cell death, including ferroptosis.

Ferroptosis is a new type of cell death where Fe^{2+}, $^{\bullet}OH$, and lipid peroxidation play crucial role [21-23]. Recently, ferroptosis was implicated in several diseases such as neuronal degeneration, kidney injury, and cancer [21, 24]. Ferroptosis is regulated by a number of genes/proteins. Glutathione peroxidase 4 (GPx4) was initially reported as a regulator of ferroptosis, however, other genes/proteins such as lipoxygenase, transferrin receptor, and frataxin were also reported as ferroptosis regulators [23, 25-27]. Although mitochondrial by-products play an important role in ferroptosis, the involvement of mitochondria in ferroptosis is currently under debate. [23, 27-29]. For example, osteosarcoma ρ^0 cells are not sensitive to erastin-induced cell death [28]. In addition, erastin and RSL3 induce cell death, even when mitochondria are depleted by parkin overexpression and carbonyl cyanide 3-chlorophenylhydrazone treatment [23]. Other reports describe a relationship among mitochondria, ferroptosis, and frataxin, a mitochondrial protein [27, 29]. However, there are few reports that ferroptosis contributes to ρ^0 cell sensitivity to H_2O_2

In the present *in vitro* study, we investigated the involvement of mitochondria in H_2O_2-induced ferroptosis and examined the molecules that regulate ferroptosis.

Materials and methods

Cell culture and mitochondrial isolation

The HeLa and SAS human cancer cell lines were obtained from the Cell Resource Center for Biomedical Research, Institute of Development, Aging and Cancer, Tohoku University, Sendai, Japan. HeLa and SAS ρ^0 cells were established by culturing cells with 50 ng/mL ethidium bromide as described previously [13]. Cells were cultured in RPMI 1640 (189-02025; Fujifilm Wako Pure Chemical Corporation, Osaka, Japan) with 10% FBS (Biological Industries, Cromwell, CT, USA), 110 μg/mL pyruvate (Sigma-Aldrich, St Louis, MO, USA), and 50 μg/mL uridine (TOKYO Chemical Industry Co. Ltd, Tokyo, Japan) in a

humidified atmosphere at 37 °C with 5% CO_2. Mitochondria were isolated from WI-38 cells (RIKEN BRC, Ibaraki Japan) using a mitochondrial isolation kit (ab110171, Abcam, Cambridge, UK) for 24 h, as described previously [30]. Then, transferred-mitochondria (Mito) cells were established by culture with 5 μg/mL isolated mitochondria. HeLa and SAS parental cells and Mito cells were cultured with RPMI 1640 with 10% FBS in a humidified atmosphere at 37 °C with 5% CO_2. Exponentially growing cells were used in all experiments.

Flow cytometry analysis

To investigate H_2O_2-induced cell death, a BD Accuri C6 Flow Cytometer (BD Biosciences, San Jose, CA, USA) was used. Briefly, 2 x 10^5 HeLa and SAS ρ^0 cells were cultured in 60 mm dishes for 24 h and treated with 75 μM (for HeLa ρ^0 cells) or 50 μM (for SAS ρ^0 cells) H_2O_2 (Nacalai Tesque, Kyoto, Japan) for 3 h. After H_2O_2 treatment, the cells were trypsinized and resuspend with 1x binding buffer (10 mM HEPES pH 7.4, 140 mM NaCl, and 2.5 mM $CaCl_2$). After filtration through a 40 μm cell strainer (352235; BD Biosciences), 1 x 10^5 cells/100 μL solutions were mixed with 4 μg/mL propidium iodide (PI; Sigma-Aldrich) and 20 μM Liperfluo (DOJINDO Laboratories, Kumamoto, Japan) or 5 μL Annexin V-FITC (4700-100; MEDICAL & BIOLOGICAL LABORATORIES CO. LTD., Aichi, Japan) at room temperature for 20 min. Then, 400 μL 1x binding buffer were added and fluorescence images were obtained.

Annexin V and Liperfluo detection by fluorescence microscopy

HeLa and SAS ρ^0 cells were cultured in glass-bottom dishes (Matsunami Glass Ind., Ltd., Osaka, Japan) with 20 μM Liperfluo or 5 μL Annexin V-FITC following H_2O_2 treatment as described above. Then, cells were washed three times with 1x binding buffer. Fluorescence images were obtained using a BZ-8000 fluorescence microscope (KEYENCE Corporation, Osaka, Japan) with a GFP-BP filter (excitation and absorption wavelengths: 470/40 nm). No autofluorescence was detected under the conditions of this experiment (Fig S1). ImageJ software (Rasband, W.S., ImageJ, U. S. National Institutes of Health, Bethesda, Maryland, USA, http://rsb.info.nih.gov/ij/, 1997–2012) was used to

162 measure fluorescence intensity.
163
164 *Intracellular and mitochondrial Fe^{2+} detection*
165 FerroOrange (Goryo Chemical Inc., Hokkaido, Japan) and Mito-FerroGreen
166 (Dojindo) were used to detect intracellular and mitochondrial Fe^{2+}. HeLa and
167 SAS ρ^0 cells were cultured overnight in glass-bottom dishes (Matsunami Glass).
168 Then, the cells were washed twice with Hank's Balanced Salt Solution (HBSS)
169 (Fujifilm Wako Pure Chemical Corporation) to remove residual FBS. The cells
170 were treated with 1 μM FerroOrange or 5 μM Mito-FerroGreen in HBSS for 30
171 min at 37 ºC. After incubation, FerroOrange and Mito-FerroGreen were removed
172 by washing three times with HBSS. Fluorescence images were obtained using a
173 BZ-8000 fluorescence microscope with GFP-BP and TRITC filters (excitation
174 and absorption wavelengths: 540/25 and 605/55 nm). ImageJ software was
175 used to measure fluorescence intensity.
176
177 *The role of iron in H_2O_2 cytotoxicity using WST assay*
178 Phenanthroline (Phe: Nacalai Tesque), deferoxamine (DFO: Sigma-Aldrich) and
179 deferasirox (DFX: Cayman Chemical, Ann Arbor, MI, USA) were used to
180 investigate the involvement of iron during H_2O_2 treatment. HeLa and SAS ρ^0
181 cells were cultured in 48 well plates. Then, 20 μM Phe, DFO, and DFX were
182 mixed with the cultured cells for 30 min, followed by 50 μM H_2O_2 for 1 h. The cell
183 survival ratio was analyzed using the water-soluble tetrazolium (WST) assay
184 using a CCK-8 assay kit (Dojindo), as previously described [14].
185
186 *Immunostaining*
187 HeLa and SAS ρ^0 cells were cultured in glass-bottom dishes. Cells were fixed
188 with 4% formaldehyde in PBS for 30 min and rinsed three times with PBS.
189 Plasma membranes were permeabilized by incubation in 95% ethanol with 5%
190 acetic acid for 10 min. After washing five times with PBS, the cells were
191 incubated for 30 min in blocking solution (5% skim milk in PBS-T; PBS with
192 0.05% Tween 20). Rabbit anti-AQP3 antibody (PA5-36552; Thermo Fisher
193 Scientific, Waltham, MA, USA; dilution factor: 1:500), rabbit anti-AQP5 antibody

194 (AQP-005; Alomone Labs, Jerusalem, Israel; dilution factor: 1:200), mouse
195 anti-AQP8 antibody (SAB1403559; Sigma-Aldrich; dilution factor: 1:200), rabbit
196 anti-gp91-phox (NOX2) antibody (07-024; EMD Millipore; dilution factor: 1:500)
197 and rabbit anti-PHB antibody (GTX32812; GeneTex, Inc. Irvine, CA, USA;
198 dilution factor: 1:1000) were used as primary antibodies. Cells were incubated at
199 4 °C overnight. Then, the cells were incubated with Alexa Fluor 488 goat
200 anti-mouse IgG, Alexa Fluor 488 goat anti-rabbit IgG, or Alexa Fluor 568 goat
201 anti-rabbit IgG (Thermo Fisher Scientific; A11001, A11008, and A11011)
202 secondary antibodies (dilution factor: 1:200, for 1 h at room temperature. A
203 BZ-8000 fluorescence microscope was used to obtain fluorescence images with
204 GFP-BP and Texas Red filters (excitation and absorption wavelengths: 560/40
205 and 630/60 nm) and ImageJ software was used to measure fluorescence
206 intensity.
207
208 *Western blotting*
209 Cells were extracted in lysis buffer (50 mM Tris-HCl pH 7.5, 150 mM NaCl, 1%
210 Nonidet P-40, 0.1% sodium deoxycholate, 1 mM sodium fluoride, 1 mM sodium
211 vanadate, and 1 mM phenylmethylsulfonyl fluoride: PMSF). A bicinchoninic acid
212 (BCA) Protein Assay Kit (Thermo Fisher Scientific) was used to estimate the
213 protein concentration. Proteins (10 μg per lane) were analyzed by SDS-PAGE
214 using a 15% polyacrylamide gel. SDS-PAGE was performed under reducing
215 conditions. Proteins were subsequently blotted on a PVDF membrane. After
216 blocking with 5% skim milk in PBS-T, the membranes were incubated with
217 primary antibodies in blocking solution [rabbit anti-AQP3, 5, NOX2, prohibitin 2
218 (PHB2), or mouse anti-AQP8]. After washing five times with PBS-T, the
219 membranes were incubated with peroxidase-conjugated anti-rabbit IgG antibody
220 or anti-mouse IgG antibodies (#7074, #7076; Cell Signaling Technology,
221 Danvers, MA, USA) at room temperature for 2 h. Immunoreactive proteins were
222 visualized with ImmunoStar Zeta (Fujifilm Wako) using a ChemiDoc XRS Plus
223 instrument (Bio-Rad Laboratories, Inc., Hercules, CA, USA). Anti-β-actin
224 antibody (NB100-56874; Novus Biologicals LLC, Centennial, CO, USA; dilution
225 factor: 1:1000) was used as loading control. All antibody dilution factors except

226 for β-actin antibody were same as immunofluorescence assays. All western blot
227 analyses were performed using an identical sample amount in each well and
228 were blotted under the same conditions.
229
230 *Immunoprecipitation*
231 Cells were suspended and homogenized with ten times volume of Homogenize
232 solution (HS; 20 mM Tris-HCl pH 7.6, 150 mM NaCl, 1% NP-40, 100 μg/mL
233 DNase, 50 μg/mL RNaseA, 1 mM PMSF, and protease inhibitor cocktail).
234 Homogenized samples were pre-incubated with Protein A-Sepharose 4B beads
235 (Sigma-Aldrich) that were previously incubated with NOX2 antibody or normal
236 rabbit IgG. An equal volume of sample (1 mg) and NOX2 or normal rabbit
237 IgG-bound beads were incubated at 4 ºC for 4 h. After the incubation, beads
238 were washed three times with HS containing 1 mg/mL BSA. The washed beads
239 were mixed with sample buffer (50 mM Tris-HCl pH 6.8, 2% SDS, 6%
240 2-mercaptoethanol, and 20% glycerol) to extract NOX2-bound proteins.
241 Extracted samples were analyzed by SDS-PAGE and western blotting as
242 described above.
243
244 *siRNA gene silencing*
245 HeLa and SAS cells were transfected with synthetic miRNA corresponding to
246 AQP3 (360-1-B, 360-2B; Bioneer, Daejeon, Korea) and AQP5, AQP8, or PHB2
247 (sc-2917, sc-42369, sc-45849; Santa Cruz Biotechnology, Dallas, TX, USA)
248 using Lipofectamine RNAiMAX Transfection Reagent (Thermo Fisher Scientific).
249 AccuTarget Negative Control siRNA (SN-1003: Bioneer) was used as a control.
250 Cell viability was measured using CCK-8 assay, as described above.
251
252 *Measurement of intracellular H_2O_2*
253 Intracellular H_2O_2 was visualized using HYDROP (Goryo Chemical Inc.) as
254 described previously [13]. Briefly, cells in glass-bottom dishes (Matsunami
255 Glass) were cultured in RPMI 1640 with 50 μM H_2O_2 for 1 h. After washing out
256 the H_2O_2 twice with RPMI 1640, the cells were treated with 2.5 μM HYDROP in
257 RPMI 1640 at 37 ºC for 20 min. Then, the cells were washed twice with RPMI

258 1640. Fluorescence images were obtained using a BZ-8000 fluorescence
259 microscope (KEYENCE) with a GFP-BP filter. ImageJ software was used to
260 measure fluorescence intensity.
261
262 *Quantitative PCR*
263 Total RNA was extracted using ISOGEN reagent (Nippon Gene Toyama, Japan).
264 The quality of RNA was checked by absorbance and electrophoresis. All cDNAs
265 were prepared by reverse transcription of 1 μg total RNA using oligo dT (20)
266 primer (0.4 μM/50 μl final volume) and ReverTra Ace (TOYOBO CO Ltd., Osaka,
267 Japan). After 10x dilution with Tris-EDTA buffer (TE: 10 mM Tris-HCl pH 8.0, 1
268 mM EDTA), 0.5 μL cDNA (equivalent to 1 ng total RNA) was used for quantitative
269 polymerase chain reaction (qPCR). The qPCR reactions were performed using
270 an Applied Biosystems 7300 instrument (Applied Biosystems; Foster City, CA,
271 USA) using TUNDERBIRD qPCR Mix (TOYOBO). *β-actin* was used as the
272 loading control. cDNA was amplified as follows: one cycle at 95 °C for 10 min,
273 followed by 40 cycles of 95 °C for 10 s and 60 °C for 60 s. Each experiment was
274 performed in triplicate. Table 1 shows the primer sequences used in this
275 experiment.
276
277 *Data analysis*
278 Relative fluorescence intensities were obtained by measuring the fluorescence
279 intensity of each cell using all the cells from three independent dishes.
280 Fluorescence was normalized by subtracting the background fluorescence
281 intensity of each dish from the fluorescence intensity of each cell. One-way
282 ANOVA with Scheffe's F test was performed for the WST assay. All other
283 statistical analyses were performed using Student's *t*-test. $p < 0.05$ was
284 considered statistically significant. The results are expressed as means ±
285 standard error.
286
287 **Results**
288
289 *Induction of ferroptosis by H_2O_2 treatment in ρ^0 cells*

290 To determine whether H_2O_2-mediated cell death occurs via apoptosis or
291 ferroptosis, the cells were treated with Liperfluo or Annexin V and PI followed by
292 flow cytometry analysis. Liperfluo is a ferroptosis marker [31] and Annexin V is
293 an apoptosis marker. Our results showed that Liperfluo increased more than
294 Annexin V in both HeLa and SAS ρ^0 cells after 3-h H_2O_2 treatment (1.55 vs.
295 1.15-fold in HeLa ρ^0 cells and 3.79 vs 1.63-fold in SAS ρ^0 cells, Fig. 1A).
296 Moreover, similar results were detected using fluorescence microscopy (Fig. 1B).
297 Indeed, Liperfluo labeling intensity increased significantly after 3 h of H_2O_2
298 treatment in both HeLa and SAS ρ^0 cells. In contrast, the intensity of Annexin V
299 labeling increased slightly, but it was not significant (Fig. 1C). These results
300 strongly suggest that cell death after H_2O_2 treatment occurs via ferroptosis, and
301 that cell death occurs relatively quickly.
302
303 *Fe^{2+} amount is involved in H_2O_2-induced cell death in ρ^0 cells*
304 Intracellular and mitochondrial Fe^{2+} levels and the effect of iron chelators were
305 examined to investigate the involvement of Fe^{2+} during H_2O_2 sensitivity in ρ^0
306 cells. Intracellular Fe^{2+} was measured using FerroOrange (Fig. 2A, B) and
307 mitochondrial Fe^{2+} was measured using Mito-FerroGreen (Fig. 2C, D). Both
308 intracellular and mitochondrial Fe^{2+} in ρ^0 cells were significantly higher than in
309 parental cells. We confirmed that the Mito-FerroGreen signal originated from
310 mitochondria using Mito-Tracker red CMXRos (Fig. S2). No significant
311 differences were detected in the number of mitochondria in each cell between
312 parental cells and ρ^0 cells (see details in discussion).
313 We examined whether iron chelators could recover H_2O_2 sensitivity. The typical
314 iron chelators, Phe, DFO, and DFX, were used. Phe and DFX treatment
315 significantly reduced cell death caused by H_2O_2 treatment (Fig. 2E).
316
317 *Upregulation of AQPs in ρ^0 cells*
318 The spatial distribution of AQPs in ρ^0 cells was investigated because some
319 AQPs allow H_2O_2 flux. In both HeLa and SAS ρ^0 cells, the expression of AQP 3,
320 5, and 8, which were reported to pass H_2O_2, was higher than in parental cells.
321 The expression of AQPs in ρ^0 cells was strongly observed at the cell margin, i.e.
322 the plasma membrane (Fig. 3). We further investigated the amount of AQP

323 protein by Western blot. AQP3, 5, and 8 expression was upregulated in both
324 HeLa and SAS ρ^0 cells (Fig. 4A).
325
326 *Interaction between AQPs and NOX2*
327 To investigate whether AQPs directly bind to NOX2, immunoprecipitation
328 experiments were performed. We observed that AQP3, 5, and 8 bind to NOX2
329 (Fig. 4A). Next, we investigated the spatial distribution of NOX2 by fluorescence
330 microscopy. NOX2 was detected in nuclei and in the plasma membrane (Fig. 4B).
331 Stronger intensity of NOX2 was detected in both HeLa and SAS ρ^0 cells
332 compared with parental cells (Fig. 4C).
333
334 *AQP knockdown abolishes H_2O_2-induced ferroptosis*
335 To investigate whether AQP3, 5, and 8 are involved in H_2O_2 sensitivity, we
336 knocked down these genes with siRNA. After AQP3, 5, and 8 knockdown with
337 specific siRNA, the cells were treated with H_2O_2 for 1 h. Cell viability was
338 measured using CCK-8 assays. The results revealed that cell viability was
339 improved by knocking down AQP3, 5, and 8 compared with negative control
340 siRNA transfection. Internal H_2O_2 amount was also measured by HYDROP after
341 H_2O_2 treatment. Our results show that the internal H_2O_2 amount was significantly
342 decreased after siAQP treatment (Fig. 5C, D).
343
344 *Transfer of normal mitochondria reduces H_2O_2 sensitivity in ρ^0 cells*
345 To clarify the relationship between mitochondrial function and AQP expression,
346 isolated normal mitochondria were transferred into ρ^0 cells (Mito cells). After
347 confirming that normal mitochondria were transferred into ρ^0 cells, AQP
348 expression, H_2O_2 sensitivity, and Fe^{2+} levels were investigated. In the Mito cells,
349 AQP3, 5, and 8 expression (Fig. 6. A-C), H_2O_2 sensitivity (Fig. 6. D, E), and Fe^{2+}
350 levels (Fig. 6. F-I) were all significantly decreased. Overall, these findings
351 suggest the importance of mitochondria for H_2O_2-induced ferroptosis.
352
353 *Mitochondrial PHB2 regulates AQP expression*
354 Since PHB2 plays an important role in mitochondrial functions such as
355 membrane potential and mitochondrial morphology, PHB2 expression was

examined at the mRNA and protein levels in ρ^0 cells. PHB2 gene expression was significantly downregulated in ρ^0 cells and was rescued in Mito cells (Fig. 7A). Furthermore, significantly weaker PHB2 expression was observed in ρ^0 cells compared to parental and Mito cells using immunofluorescence microscopy (Fig. 7B, C). Western blot analysis confirmed that PHB2 expression was decreased in ρ^0 cells in comparison with parental and Mito cells (Fig. 7D).

Finally, to investigate whether PHB2 regulates AQP expression, PHB2 knockdown was performed. PHB2 knockdown upregulated AQP3, 5, and 8 gene expression (Fig. 8), indicating that PHB2 negatively regulates AQP expression.

Discussion

It has previously been reported that cell death induced by H_2O_2 treatment occurs via apoptosis or necroptosis [32]. However, in our present study, ferroptosis occurred in ρ^0 cells at a relatively early stage after H_2O_2 treatment. Notably, H_2O_2-induced ferroptosis was recently reported in rat glioma cells [33]. The induction of apoptosis by H_2O_2 treatment was confirmed by costaining with Annexin V and PI (early apoptosis is stained by only Annexin V and late apoptosis is stained with Annexin V and PI). The induction of ferroptosis was confirmed with Liperfluo and PI. As a result, more Liperfluo-positive cells were observed than Annexin V-positive cells 3 h after H_2O_2 treatment, confirming the induction of ferroptosis after H_2O_2 (Fig.1, Fig.S3). Interestingly, treating ρ^0 cells with H_2O_2 for 2 h downregulated the key apoptotic genes Caspase 8 and 9 (Fig. S4). Furthermore, the GPx4 gene, which acts as a suppressor of lipid peroxidation and ferroptosis [21, 34], was not upregulated in ρ^0 cells 2 h after H_2O_2 treatment. However, in parental cells, GPx4 expression was upregulated 2 h after H_2O_2 treatment (Fig.S4). These results highlight the involvement of mitochondria in the ferroptosis process. Furthermore, nuclear factor erythroid 2-related factor 2 (Nrf2) contributes in regulation of GPx4 gene expression [35], however, its gene expression was suppressed in ρ^0 cells (Fig.S5). The nuclear factor erythroid 2–related factor 2 (Nrf2)-Kelch-like ECH-associated protein 1 (keap1) pathway enables the upregulation of antioxidant enzymes such as GPx4, but does not work in ρ^0 cells. It seems that the promotion of ferroptosis occurs

differently than apoptosis during the early stage of H_2O_2 treatment, at least in ρ^0 cells. However, more studies are necessary to develop our understanding about the mechanism of ferroptosis induction after H_2O_2 treatment.

Ferroptosis is cell death from iron-dependent lipid peroxidation. ρ^0 cells are sensitive to H_2O_2-mediated cell death because ρ^0 cells are susceptible lipid peroxidation compared to parental cells [14]. However, the importance of the intracellular Fe^{2+} content has not yet been addressed. Our findings reveal that both intracellular and mitochondrial Fe^{2+} were significantly increased in ρ^0 cells. Interestingly, when endogenous Fe^{2+} was suppressed by iron chelators, H_2O_2 sensitivity was ameliorated (Fig. 2E, F). The effect of DFO was limited, likely because it is water-soluble and does not penetrate the plasma membrane. Collectively, our results indicate that H_2O_2 sensitivity in ρ^0 cells is due to increased ferroptosis.

It has previously been reported that ferroptosis occurs by lipid peroxidation of the plasma membrane. The lipid peroxidation of the plasma membrane occurs by $^{\bullet}OH$ that results from the “Fenton reaction,” where H_2O_2 reacts with Fe^{2+}. The amount of $^{\bullet}OH$ and lipid peroxidation is initially higher in ρ^0 cells than in parental cells [14]. H_2O_2 enters ρ^0 cells more readily when treated with H_2O_2 compared to parental cells [13]. It has also been reported that AQP3, 5, and 8 expressed on the plasma membrane also regulate the permeability of the extracellular H_2O_2 via H_2O_2 channel activity [16-18]. Therefore, we examined the spatial and quantitative expression of AQP3, 5, and 8 in the present study. Indeed, AQP3, 5, and 8 expression was enhanced in ρ^0 cells according to both immunostaining and Western blot analysis (Fig. 3, 4A). AQP8 and NOX2 directly interact, and H_2O_2 produced by NOX2 enters cells via AQP8 [36]. Therefore, an immunoprecipitation experiment was performed to investigate whether AQPs bind to NOX2 directly. Our results indicate that NOX2 expression is upregulated in ρ^0 cells, and that NOX2 binds to AQP3, 5, and 8 in both HeLa and SAS cells (Fig. 4). Furthermore, knockdown of AQP3, 5, and 8 increased cell viability after H_2O_2 treatment and decreased the amount of endogenous H_2O_2 (Fig.5, Fig.S6). When H_2O_2 is administered to ρ^0 cells, lipid peroxidation in the plasma membrane is enhanced, leading to increased ferroptosis because intracellular

H_2O_2, AQP and NOX expression, and Fe^{2+} levels are higher in ρ^0 cells than in parental cells. Together, these factors would produce more •OH. These results indicate that drugs that enhance AQP expression may be effective in cancer treatment. Candidates that enhance AQP expression are vasopressin, epidermal growth factor (EGF), the Chinese herb “Keigai”, and nuclear receptor estrogen receptor α (ERα). Vasopressin, an antidiuretic hormone, enhances AQP2 expression in the kidney [37], EGF increases AQP3 expression in MPC-83 pancreatic cancer [38], and the Chinese herb “Keigai” enhances AQP3 expression [39]. Furthermore, ERα up-regulates AQP7 expression [40]. However, further investigations will be needed to address some questions, including whether vasopressin or ERα activate AQP3, 5, and 8 and promote H_2O_2 permeability in the plasma membrane. The combination of these candidate molecules with anti-cancer agents or radiation might lead to more effective cancer treatment.

To verify whether enhanced AQP expression and H_2O_2 sensitivity in ρ^0 cells are due to mitochondrial dysfunction, mitochondria transfer experiments were performed. As a result, mitochondrial transfer reduced the expression of AQP3, 5, and 8, and rescued cellular sensitivity to H_2O_2. In addition, mitochondrial transfer decreased intracellular and mitochondrial Fe^{2+} levels (Fig. 6). We speculate that mitochondrial dysfunction causes enhanced mitochondrial membrane permeability by AQPs, produces more ROS by the Fenton reaction, and induces leak of Fe^{2+} from mitochondrial interior, leading to cell death via ferroptosis. Therefore, it may be possible to extract mitochondria after establishing ρ^0 cells from the patient’s own tissue and introduce them into cancer cells that have normal mitochondria, which could offer a new treatment to increase cellular sensitivity to ROS and drugs. We believe that mitochondria transfer might be an effective therapeutic strategy in the near future. However, mitochondria transfer is only in the initial development stage, so further investigation is needed to clarify technical and ethical issues.

PHB2 is an important protein for maintaining mitochondrial function. Indeed, PHB2 is expressed in mitochondria, and is also present in the cytoplasm,

nucleus, and plasma membrane, and controls various functions [41, 42]. For example, PHB2 maintains mitochondrial morphology and controls mitophagy [43]. Further, PHB2 regulates the cell cycle and cytoplasmic signaling pathways [44, 45]. PHB2 is also involved in transcriptional regulation with ERα in the nucleus [46]. On the plasma membrane, PHB2 controls insulin signaling by binding to the insulin receptor, and protects against viral infections such as coronavirus. [47]. Our results indicate that the expression of PHB2 in the parental, ρ^0, and Mito cells is different and is downregulated in ρ^0 cells. Furthermore, knocking down PHB2 with siRNA in the parental cells enhances AQP expression (Fig. 7, 8). Since the PHB2 gene was not rescued by AQP knockdown (Fig.S7), it is likely that PHB2 downregulates AQP gene expression. PHB2 translocates to the nucleus with ERα in HeLa and MCF-7 cells and represses ERα-dependent transcription [46, 48]. Moreover, ERα up-regulates AQP expression, as mentioned in the Results section [41]. From these results, we propose that mitochondrial PHB2 plays an important role in the regulation of ROS sensitivity by downregulating AQP expression, probably through nuclear receptors such as ERα.

PHB2 functions as a putative membrane scaffold in mitochondria and stabilizes phospholipids such as cardiolipin in the inner mitochondrial membrane [49]. Knockdown of PHB2 produces more intracellular ROS, reduces adipogenesis, and reduces lipid accumulation in 3T3-L1 cells [50]. Furthermore, the depletion of PHB2 promotes fatty acid oxidation and decreases fatty acid uptake in cardiomyocytes [51]. We previously reported that ROS generation and lipid peroxidation in ρ^0 cells is higher than in parental cells. The expression of lipoxygenase, an enzyme that oxidizes fatty acids, is also higher than in parental cells [14]. In this study, we showed low PHB2 expression and high Fe^{2+} content in ρ^0 cells, and showed that mitochondrial transfer rescues this condition. Oxidative stress such as selenite treatment leads to iron-sulfur cluster degradation and increases Fe^{2+} levels in mitochondria followed by lipid peroxidation [52]. These damaged mitochondria are degraded and the mitochondrial contents, including Fe^{2+}, are released into the cytoplasm for degradation in lysosomes [53]. It has been reported that mitochondria morphology is different between parental and ρ^0 cells, but the total mitochondrial

volume is similar [54, 55]. We confirmed that the volume of mitochondria was not significantly different among parent, ρ^0, and Mito cells (Fig. S8). When the morphology of mitochondria in ρ^0 cells was observed by confocal microscopy and transmission electron microscopy, the network structure appeared disrupted, the mitochondrial appeared swollen, the matrix appeared to be electron-empty, and structure of cristae was destroyed [54]. Taken together, these results indicate that the downregulation of PHB2 by mitochondrial dysfunction leads to decreased fatty acid turnover and increased Fe^{2+} contents, failing to rescue the lipid peroxidation that leads to cell death. Therefore, downregulating PHB2 expression could create a ROS-sensitive condition, which may enable more effective cancer treatment.

In this study, we showed that H_2O_2 mediates ferroptosis in ρ^0 cells. Mitochondrial dysfunction, such as mtDNA depletion and conditions such as decreased PHB2, leads to more ferroptosis because mitochondrial dysfunction, like PHB2 reduction, increases intracellular H_2O_2, AQP, NOX, and Fe^{2+} levels, and could result in increased $^{\bullet}OH$ production, resulting in lipid peroxidation (summarized in Fig. 9). Some anti-cancer agents kill cancer cells through the production of ROS. Furthermore, H_2O_2 is used as a sensitizer in cancer treatment. Therefore, amplifying AQP expression before sensitizer treatment will likely enhance the therapeutic effect. Further progress in this field will likely facilitate improved cancer treatment.

Acknowledgments

This work was supported by a Grant from the Kodama Memorial Fund for Medical Research to K.T. and JSPS KAKENHI (Grant-in Aid for Scientific Research C: No. 18K09772 to Y.T.; 19K10318 to K.T.).

Conflicts of interest

The authors declare no conflicts of interest.

515 **References**

516 [1] S. Tada-Oikawa, S. Oikawa, M. Kawanishi, M. Yamada, S. Kawanishi,
517 Generation of hydrogen peroxide precedes loss of mitochondrial
518 membrane potential during DNA alkylation-induced apoptosis, FEBS Lett.
519 442 (1999) 65-69. https://doi.org/10.1016/s0014-5793(98)01618-4.
520 [2] G. Varbiro, B. Veres, F. Jr. Gallyas, B. Sumegi, Direct effect of Taxol on free
521 radical formation and mitochondrial permeability transition, Free Radic. Biol.
522 Med. 31 (2001) 548-558. https://doi.org/10.1016/s0891-5849(01)00616-5.
523 [3] M. Murata, T. Suzuki, K. Midorikawa, S. Oikawa, S. Kawanishi, Oxidative
524 DNA damage induced by a hydroperoxide derivative of cyclophosphamide,
525 Free Radic. Biol. Med. 37 (2004) 793-802.
526 https://doi.org/10.1016/j.freeradbiomed.2004.05.009.
527 [4] D. Magda, R.A. Miller, Motexafin gadolinium: a novel redox active drug for
528 cancer therapy, Semin. Cancer Biol. 16 (2006) 466-476.
529 http://doi.org/10.1016/j.semcancer.2006.09.002
530 [5] J. Alexandre, C. Nicco, C. Chéreau, A. Laurent, B. Weill, F. Goldwasser, F.
531 Batteux, Improvement of the therapeutic index of anticancer drugs by the
532 superoxide dismutase mimic mangafodipir, J. Natl. Cancer Inst. 98 (2006)
533 236-244. https://doi.org/10.1093/jnci/djj049.
534 [6] Y. Fang, B.J. Moore, Q. Bai, K.M. Cook, E.J. Herrick, M.B. Nicholl, Hydrogen
535 peroxide enhances radiation-induced apoptosis and inhibition of melanoma
536 cell proliferation, Anticancer Res. 33 (2013) 1799-1807.
537 [7] S. Kariya, K. Sawada, T. Kobayashi, T. Karashima, T. Shuin, A. Nishioka, Y.
538 Ogawa, Combination treatment of hydrogen peroxide and X-rays induces

539 apoptosis in human prostate cancer PC-3 cells, Int. J. Radiat. Oncol. Biol.
540 Phys. 75 (2009) 449-454. http:// doi.org/10.1016/j.ijrobp.2009.04.092.
541 [8] B. Halliwell, J.M.C. Gutterridge, Oxygen free radicals and iron in relation to
542 biology and medicine: some problems and concepts, Arch. Biochem.
543 Biophys. 246 (1986) 501-514.
544 http://doi.org/10.1016/0003-9861(86)90305-x.
545 [9] H.P. Indo, M. Davidson, H-C. Yen, S. Suenaga, K. Tomita, T. Nishii, M.
546 Higuchi, Y. Koga, T. Ozawa, H.J. Majima, Evidence of ROS generation by
547 mitochondria in cells with impaired electron transport chain and
548 mitochondrial DNA damage, Mitochondrion 7 (2007) 106-118.
549 http://doi.org/10.1016/j.mito.2006.11.026.
550 [10] A. Ogura, S. Oowada, Y. Kon, A. Hirayama, H. Yasui, S. Meike, S.
551 Kobayashi, M. Kuwabara, O. Inanami, Redox regulation in
552 radiation-induced cytochrome c release from mitochondria of human lung
553 carcinoma A549 cells, Cancer Lett. 277 (2009) 64e71.
554 http://doi.org/10.1016/j.canlet.2008.11.021
555 [11] A. Chatterjee, E. Mambo, D. Sidransky, Mitochondrial DNA mutations in
556 human cancer, Oncogene 25 (2006) 4663-4674.
557 http://doi.org/10.1038/sj.onc.1209604.
558 [12] M.T. Lin, M.F. Beal. Mitochondrial dysfunction and oxidative stress in
559 neurodegenerative diseases, Nature 443 (2003) 787-795.
560 http://doi.org/10.1038/nature05292.
561 [13] K. Tomita, Y. Kuwahara, Y. Takashi, T. Tsukahara, A. Kurimasa, M.
562 Fukumoto, Y. Nishitani, T. Sato, Sensitivity of mitochondrial DNA depleted

ρ0 cells to H_2O_2 depends on the plasma membrane status, Biochem. Biophys. Res. Commun. 490 (2017) 330-335. http://doi.org/10.1016/j.bbrc.2017.06.044.

[14] K. Tomita, Y. Takashi, Y. Ouchi, Y. Kuwahara, K. Igarashi, T. Nagasawa, H. Nabika, A. Kurimasa, M. Fukumoto, Y. Nishitani, T. Sato, Lipid peroxidation increases hydrogen peroxide permeability leading to cell death in cancer cell lines that lack mtDNA, Cancer Sci. 110 (2019) 2856. http://doi.org/10.1111/cas.14132.

[15] Y. Takashi, K. Tomita, Y. Kuwahara, H. Nabika, K. Igarashi, T. Nagasawa, A. Kurimasa, M. Fukumoto, Y. Nishitani, T. Sato, Data on the aquaporin gene expression differences among ρ^0, clinically relevant radioresistant, and the parental cells of human cervical cancer and human tongue squamous cell carcinoma, Data Brief, 20 (2018) 402-410. http://doi.org/10.1016/j.dib.2018.08.025.

[16] E.W. Miller, B.C. Dickinson, C.J. Chang, Aquaporin-3 mediates hydrogen peroxide uptake to regulate downstream intracellular signaling, Proc. Natl. Acad. Sci. U.S.A. 107 (2010) 15681-15686. http://doi.org/10.1073/pnas.1005776107.

[17] C. Rodrigues, C. Pimpão, A.F. Mósca, A.S. Coxixo, D. Lopes, I. V. da Silva, P.A. Pedersen, F. Antunes, G. Soveral, Human aquaporin-5 facilitates hydrogen peroxide permeation affecting adaption to oxidative stress and cancer cell migration, Cancers (Basel) 11 (2019) 932. http://doi.org/10.3390/cancers11070932.

[18] G.P. Bienert, A.L. Moller, K.A. Kristiansen, A. Schulz, I.M. Moller, J.K.

Schjoerring, T.P. Jahn, Specific aquaporins facilitate the diffusion of hydrogen peroxide across membranes, J. Biol. Chem. 282 (2007) 1183-1192. http://doi.org/10.1074/jbc.M603761200.

[19] R. Beri, R. Chandra, Chemistry and biology of heme. Effect of metal salts, organometals, and metalloporphyrins on heme synthesis and catabolism, with special reference to clinical implications and interactions with cytochrome P-450, Drug Metab. Rev. 25 (1993) 49-152. http://doi.org/10.3109/03602539308993973.

[20] D.C. Johnson, D.R. Dean, A.D. Smith, M.K. Johnson, Structure, function, and formation of biological iron-sulfur clusters, Annu. Rev. Biochem. 74 (2005) 247-281. http://doi.org/10.1146/annurev.biochem.74.082803.133518.

[21] B.R. Stockwell, J.P.F Angeli, H. Bayir, A.I. Bush, M. Conrad, S.J. Dixon, S. Fulda, S. Gascón, S.K. Hatzios, V.E. Kagan, K. Noel, X. Jiang, A. Linkermann, M.E. Murphy, M. Overholtzer, A. Oyagi, G.C. Pagnussat, J. Park, Q. Ran, C.S. Rosenfeld, K. Salnikow, D. Tang, F.M. Torti, S.V. Torti, S. Toyokuni, K.A. Woerpel, D.D. Zhang, Ferroptosis: A regulated cell death nexus linking metabolism, redox biology, and disease, Cell 171 (2017) 273-285. https://doi.org/10.1016/j.cell.2017.09.021.

[22] L. Jiang, N. Kon, T. Li, S.J. Wang, T. Su, H. Hibshoosh, R. Baer, W. Gu, Ferroptosis as a p53-mediated activity during tumour suppression, Nature 520 (2015) 57-62. https://doi.org/10.1038/nature14344.

[23] S.J. Dixon, K.M. Lemberg, M.R. Lamprecht, R. Skouta, E.M. Zaitsev, C.E. Gleason, D.N. Patel, A.J. Bauer, A.M. Cantley, W.S. Yang, B.3rd Morrison,

611 B.R. Stockwell, Ferroptosis: an iron-dependent form of nonapoptotic cell
612 death, Cell 149 (2012) 1060-1072.
613 https://doi.org/10.1016/j.cell.2012.03.042.
614 [24] C.M. Bebber, F. Müller, L.P. Clemente, J. Weber, S. von Karstedt,
615 Ferroptosis in cancer cell biology, Cancers (Basel) 12 (2020) 164.
616 http://doi.org/10.3390/cancers12010164.
617 [25] S.E. Wenzel, Y.Y. Tyurina, J. Zhao, C.M. St Croix, H.H. Dar, G. Mao, V.A.
618 Tyurin, T.S. Anthonymuthu, A.A. Kapralov, A.A. Amoscato, K.
619 Mikulska-Ruminska, I.H. Shrivastava, E.M. Kenny, Q. Yang, J.C.
620 Rosenbaum, L.J. Sparvero, D.R. Emlet, X. Wen, Y. Minami, F. Qu, S.C.
621 Watkins, T.R. Holman, A.P. VanDemark, J.A. Kellum, I. Bahar, H. Bayır, V.E.
622 Kagan, PEBP1 wardens ferroptosis by enabling lipoxygenase generation of
623 lipid death signals, Cell 171 (2017) 628-641.
624 http://doi.org/10.1016/j.cell.2017.09.044.
625 [26] H. Feng, K. Schorpp, J. Jin, C.E. Yozwiak, B.G. Hoffstrom, A.M.Decker, P.
626 Rajbhandari, M.E. Stokes, H.G. Bender, J.M. Csuka, P.S. Upadhyayula, P.
627 Canoll, K. Uchida, R.K. Soni, K. Hadian, B.R. Stockwell, Transferrin
628 receptor is a specific ferroptosis marker, Cell Rep. 30 (2020) 3411-3423.
629 http://doi.org/10.1016/j.celrep.2020.02.049.
630 [27] J. Du, Y. Zhou, Y. Li, J. Xia, Y. Chen, S. Chen, X. Wang, W. Sun, T. Wang, X.
631 Ren, X. Wang, Y. An, K. Lu, W. Hu, S. Huang, J. Li, X. Tong, Y. Wang,
632 Identification of frataxin as a regulator of ferroptosis, Redox Biol. 32 (2020)
633 101483. http://doi.org/10.1016/j.redox.2020.101483.
634 [28] M.M. Gaschler, F. Hu, H. Feng, A. Linkermann, W. Min, B.R. Stockwell,

Determination of the subcellular localization and mechanism of action of ferrostatins in suppressing ferroptosis, ACS Chem. Biol. 13 (2018) 1013-1020, https://doi.org/10.1021/acschembio.8b00199.

[29] H. Wang, C. Liu, Y. Zhao, G. Gao, Mitochondria regulation in ferroptosis, Eur. J. Cell Biol. 99 (2020) 151058. http://doi.org/10.1016/j.ejcb.2019.151058.

[30] A.M. Roushandeh, K. Tomita, Y. Kuwahara, A. Jahanian-Najafabadi, K. Igarashi, M.H. Roudkenar, T. Sato, Transfer of healthy fibroblast-derived mitochondria to HeLa ρ^0 and SAS ρ^0 cells recovers the proliferation capabilities of these cancer cells under conventional culture medium, but increases their sensitivity to cisplatin-induced apoptotic death, Mol. Biol. Rep. 2020 *in press*. http://doi.org/10.1007/s11033-020-05493-5.

[31] B.R. Stockwell, X. Jiang, The chemistry and biology of ferroptosis, Cell Chem. Biol. 27 (2020) 365-375. https://doi.org/10.1016/j.chembiol.2020.03.013.

[32] J. Xiang, C. Wan, R. Guo, D. Guo, Is hydrogen peroxide a suitable apoptosis inducer for all cell types?, Biomed. Res. Int. (2016) 7343965. http://doi.org/10.1155/2016/7343965.

[33] T. Jiang, J. Chu, H. Chen, H. Cheng, J. Su, X. Wang, Y. Cao, S. Tian, Q. Li, Gastrodin inhibits H_2O_2-induced ferroptosis through its antioxidative effect in rat glioma cell line C6, Biol. Pharm. Bull. 43 (2020) 480-487. http://doi.org/10.1248/bpb.b19-00824.

[34] H. Imai, M. Matsuoka, T. Kumagai, T. Sakamoto, T. Koumura, Lipid peroxidation-dependent cell death regulated by GPx4 and ferroptosis, In: Nagata S., Nakano H. (eds) Apoptotic and Non-apoptotic Cell Death. Curr.

659 Top. Microbiol. Immunol. 403 (2017) 143-170. Springer, Cham.
660 http://doi.org/10.1007/82_2016_508.
661 [35] M. Dodson, R. Castro-Portuguez, D.D. Zhang, NRF2 plays a critical role in
662 mitigating lipid peroxidation and ferroptosis, Redox Biology 23 (2019)
663 101107. http://doi.org/10.1016/j.redox.2019.101107
664 [36] M. Bertolotti, G. Farinelli, M. Galli, A. Aiuti, R. Sitia, AQP8 transports
665 NOX2-generated H_2O_2 across the plasma membrane to promote signaling
666 in B cells, J. Leukoc. Biol. 100 (2016) 1071-1079.
667 http://doi.org/10.1189/jlb.2AB0116-045R.
668 [37] K. Eto, Y. Noda, S. Horikawa, S. Uchida, S. Sasaki, Phosphorylation of
669 aquaporin-2 regulates its water permeability J. Biol. Chem. 285 (2010)
670 40777-40784. http://doi.org/10.1074/jbc.M110.151928.
671 [38] L. Weijun, K. Wang, K. Gong, X. Li, K. Luo, Epidermal growth factor
672 enhances MPC-83 pancreatic cancer cell migration through the
673 upregulation of aquaporin 3, Mol. Med. Rep. 6 (2012) 607-610.
674 http://doi.org/10.3892/mmr.2012.966.
675 [39] Y. Isohama, Increase in aquaporin 3 expression in keratinocytes by
676 *Schizonepeta tenuifolia* (in Japanese), Folia. Pharmacol. Jpn. 143 (2014)
677 115-119. https://doi.org/10.1254/fpj.143.115.
678 [40] X. Fu, J. Zhu, L. Zhang, J. Shu, Long non-coding RNA NEAT1 promotes
679 steatosis via enhancement of estrogen receptor alpha-mediated AQP7
680 expression in HepG2 cells, Artif. Cells Nanomed. Biotechnol. 47 (2019)
681 1782-1787. http://doi.org/10.1080/21691401.2019.1604536.
682 [41] F. Thuaud, N. Ribeiro, C.G. Nebigil, L. Désaubry, Prohibitin ligands in cell

683 death and survival: Mode of action and therapeutic potential, Chem. Biol.
684 20 (2013) 316-331. http://doi.org/10.1016/j.chembiol.2013.02.006.
685 [42] A. Bavelloni, M. Piazzi, M. Raffini, I. Faenza, W.L. Blalock, Prohibitin 2: At a
686 communications crossroads, IUBMB Life. 67 (2015) 239-254.
687 http://doi.org/10.1002/iub.1366.
688 [43] Y. Wei, W-C. Chiang, R. Sumpter Jr., P. Mishra, B Levine, Prohibitin 2 is an
689 inner mitochondrial membrane mitophagy receptor, Cell 168 (2017)
690 224-238. http://doi.org/10.1016/j.cell.2016.11.042.
691 [44] M.J. Nuell, D.A. Stewart, L. Walker, V. Friedman, C.M. Wood, G.A. Owens,
692 J.R. Smith, E.L. Schneider, R. Dell' Orco, C.K. Lumpkin, D.B. Danner, J.K.
693 McClung, Prohibitin, an evolutionarily conserved intracellular protein that
694 blocks DNA synthesis in normal fibroblasts and HeLa cells, Mol. Cell Biol.
695 11 (1991) 1372-1381. http://doi.org/10.1128/mcb.11.3.1372.
696 [45] J.W. Kim, M. Akiyama, J-H. Park, M-L. Lin, A. Shimo, T. Ueki, Y. Daigo, T.
697 Tsunoda, T. Nishidate, Y. Nakamura, T. Katagiri, Activation of
698 estrogen/estrogen receptor signaling by BIG3 through its inhibitory effect on
699 nuclear transport of PHB2/REA in breast cancer, Cancer Sci. 100 (2009)
700 1468-1478. http://doi.org/10.1111/j.1349-7006.2009.01209.x.
701 [46] K. Kasashima, E. Ohta, Y. Kagawa, H. Endo, Mitochondrial functions and
702 estrogen receptor-dependent nuclear translocation of pleiotropic human
703 prohibitin 2, J. Biol. Chem. 281 (2006) 36401-36410.
704 http://doi.org/10.1074/jbc.M605260200.
705 [47] C.T. Cornillez-Ty, L. Liao, J.R. Yates 3rd, P. Kuhn, M.J. Buchmeier, Severe
706 acute respiratory syndrome coronavirus nonstructural protein 2 interacts

with a host protein complex involved in mitochondrial biogenesis and intracellular signaling, J. Virol. 83 (2009) 10314-10318. http://doi.org/10.1128/JVI.00842-09.

[48] N-H. Kim, T. Yoshimaru, Y-A. Chen, T Matsuo, M. Komatsu, Y. Miyoshi, E. Tanaka, M. Sasa, K. Mizuguchi, T. Katagir, BIG3 inhibits the estrogen-dependent nuclear translocation of PHB2 via multiple karyopherin-alpha proteins in breast cancer cells, PLoS One 10 (2015) e0127707. http://doi.org/10.1371/journal.pone.0127707.

[49] C. Osman, M. Haag, C. Potting, J. Rodenfels, P.V. Dip, F.T. Wieland, B. Brügger, B. Westermann, T. Langercorresponding, The genetic interactome of prohibitins: coordinated control of cardiolipin and phosphatidylethanolamine by conserved regulators in mitochondria, J. Cell Biol. 184(2009) 583–596. http://doi.org/10.1083/jcb.200810189.

[50] D. Liu, Y. Lin, T. Kang, B. Huang, W. Xu, M. Garcia-Barrio, M. Olatinwo, R. Matthews, Y.E. Chen, W.E. Thompson, Mitochondrial dysfunction and adipogenic reduction by prohibitin silencing in 3T3-L1 cells, PLoS One 7 (2012) e34315. http://doi.org/10.1371/journal.pone.0034315.

[51] D. Wu, C Jian, Q. Peng, T. Hou, K. Wu, B. Shang, M. Zhao, Y. Wang, W. Zheng, Q. Ma, C-Y. Li, H. Cheng, X. Wang, L. Zhao, Prohibitin 2 deficiency impairs cardiac fatty acid oxidation and causes heart failure, Cell Death Dis. 11 (2020) 181. http://doi.org/10.1038/s41419-020-2374-7.

[52] V. Scalcon, F. Tonolo, A. Folda, A. Bindoli, M.P. Rigobello, Dimers of glutaredoxin 2 as mitochondrial redox sensors in selenite-induced oxidative stress. Metallomics 11 (2019) 1241-1251.

731 http://doi.org/10.1039/c9mt00090a.
732 [53] I. Kim, S. Rodriguez-Enriquez, J.J. Lemasters, Selective degradation of
733 mitochondria by mitophagy. Arch. Biochem. Biophys. 462 (2007) 245-253.
734 http://doi.org/10.1016/j.abb.2007.03.034.
735 [54] A. Kuka, C. Kukat, J. Brocher, I Schäfer, G. Krohne, I.A. Trounce, G. Villani,
736 P. Seibel. Generation of rho0 cells utilizing a mitochondrially targeted
737 restriction endonuclease and comparative analyses. Nucleic Acids Res. 36
738 (2008) e44. http://doi.org/10.1093/nar/gkn124.
739 [55] R.W. Gilkerson, D.H. Margineantu, R.A. Capaldi, J.M. Selker. Mitochondrial
740 DNA depletion causes morphological changes in the mitochondrial
741 reticulum of cultured human cells. FEBS Lett. 474 (2000) 1-4.
742 http://doi.org/10.1016/s0014-5793(00)01527-1.
743

744 **Figure legends**

745

746 **Fig. 1. Detection of H_2O_2-induced ferroptosis in ρ^0 cells.**

747 To investigate H_2O_2-induced cell death, cells were stained with Liperfluo (a
748 ferroptosis marker) or Annexin V (an apoptosis marker) and analyzed by flow
749 cytometry. **A:** Liperfluo expression increased after 3-h H_2O_2 treatment. However,
750 Annexin V did not increase. The concentration of H_2O_2 was 75 μM (for HeLa ρ^0
751 cells) or 50 μM (for SAS ρ^0 cells). **B:** Apoptosis and ferroptosis detected by
752 fluorescence microscopy. Liperfluo or Annexin V was used to detect ferroptosis
753 or apoptosis after H_2O_2 treatment. The conditions for H_2O_2 treatment were the
754 same as in A. **C**: Relative intensity of Liperfluo or Annexin V. **: $p < 0.01$ using
755 Student's *t*-test (vs. negative control: N.C.).

756

757 **Fig. 2. Effect of Fe^{2+} on H_2O_2 treatment in ρ^0 cells.**

758 To investigate the involvement of Fe^{2+} during H_2O_2 treatment in ρ^0 cells,
759 intracellular and mitochondrial Fe^{2+} and the effect of iron chelators were
760 examined. **A:** Detection of intracellular Fe^{2+} levels by FerroOrange. **B:** Relative
761 intensity of FerroOrange. **C:** Detection of mitochondrial Fe^{2+} by Mito-FerroGreen.
762 **D:** Relative intensity of Mito-FerroGreen. The FerroOrange and Mito-FerroGreen
763 signals in ρ^0 cells were significantly higher than in parental cells. **: $p < 0.01$
764 using Student's *t* test (vs. parent). **E** and **F:** Effect of iron chelators to H_2O_2
765 treatment in HeLa (**E**) and SAS (**F**) ρ^0 cells. Iron chelating suppressed
766 H_2O_2-induced cell death. **Phe:** Phenanthroline, **DFO:** Deferoxamine, **DFX:**
767 Deferasirox. *: $p < 0.05$, **: $p < 0.01$ using Scheffe's F test (vs. H_2O_2).

768

769 **Fig. 3. Spatial distribution of AQPs that function as H_2O_2 channels.**

770 Immunostaining of AQPs was performed to investigate the contribution of AQPs
771 to H_2O_2 permeability. **A:** Immunostaining of AQP3 in HeLa and SAS ρ^0 cells. **B:**
772 Relative fluorescence intensity of AQP3 in HeLa and SAS ρ^0 cells. **C:**
773 Immunostaining of AQP5. **D:** Relative intensity of AQP5. **E:** Immunostaining of
774 AQP8. **F:** Relative fluorescence intensity of AQP8. In HeLa and SAS ρ^0 cells,
775 AQPs were strongly expressed in the plasma membrane, and average
776 expression intensities were significantly higher than in parental cells. **: $p < 0.01$

using Student's *t*-test (vs. parent).

Fig. 4. AQP3, 5, and 8 directly bind to NOX2, which produces H_2O_2 in the cell.

Western blot analysis of AQPs was performed to investigate protein expression, and immunoprecipitation was performed to confirm if AQP and NOX2 directly interact. **A:** Western blot and immunoprecipitation of AQPs and NOX2. AQP3, 5, and 8 directly bound with NOX2. To investigate the spatial distribution of NOX2, immunostaining was also performed. **B:** Immunostaining of NOX2 in HeLa and SAS ρ^0 cells. **C:** Relative fluorescence intensity of NOX2 in HeLa and SAS ρ^0 cells. NOX2 expression was significantly higher than in parental cells. **: $p < 0.01$ using Student's *t*-test (vs. parent).

Fig. 5. AQP knockdown rescues H_2O_2 sensitivity by reducing internal H_2O_2.

To investigate the involvement of AQPs in H_2O_2 sensitivity, AQPs were knocked down by siRNA. **A:** Changes in H_2O_2 sensitivity after siAQP treatment in HeLa ρ^0 cells. The cell viability results for Negative Control (N.C.) vs. siAQP are summarized in Table 2. **B:** Changes in H_2O_2 sensitivity after siAQP treatment in SAS ρ^0 cells. **C:** Internal H_2O_2 amount visualized by HYDROP after 50 μM H_2O_2 treatment for 1 h. **D:** Relative intensity of HYDROP in HeLa and SAS ρ^0 cells. Significantly lower internal H_2O_2 levels were observed by knockdown of AQPs. **: $p < 0.01$ using Student's *t*-test (vs. N.C.).

Fig. 6. Mitochondrial transfer rescues H_2O_2 sensitivity by decreasing the expression of AQPs and reducing Fe^{2+} levels.

To clarify the relationship between mitochondrial function and AQP expression, mitochondrial transfer experiments were performed. **A-C :** AQP expression after mitochondrial transfer. **A:** AQP3. **B:** AQP5. **C:** AQP8. The expression of AQPs was significantly lower after mitochondrial transfer. **D** and **E:** Cell viability after H_2O_2 treatment. **D:** HeLa ρ^0 cells vs. HeLa Mito cells. **E:** SAS ρ^0 cells vs. SAS Mito cells. Significant H_2O_2 resistance was observed after mitochondrial transfer. **F:** Detection of intracellular Fe^{2+} by FerroOrange. **G:** Detection of mitochondrial Fe^{2+} by Mito-FerroGreen. **H:** Relative intensity of FerroOrange. **I:** Relative

810 intensity of Mito-FerroGreen. The FerroOrange and Mito-FerroGreen signals in
811 Mito cells were significantly lower after mitochondria transfer. *: $p < 0.05$, **: $p <$
812 0.01 using Student's *t*-test (vs. ρ^0 cells).
813
814 **Fig. 7. Prohibitin 2 (PHB2) expression is upregulated by mitochondrial**
815 **transfer.**
816 PHB2 expression was examined to investigate whether mitochondrial function
817 was rescued after mitochondrial transfer. **A:** PHB2 gene expression after
818 mitochondrial transfer. **B:** Immunostaining of PHB2. **C:** Relative intensity of
819 PHB2. **D:** Western blot of PHB2. PHB2 expression was lower in ρ^0 cells than in
820 parental cells. In contrast, PHB2 expression increased after mitochondrial
821 transfer. *: $p < 0.05$, **: $p < 0.01$ using Scheffe's F test.
822
823 **Fig. 8. Knockdown of PHB2 upregulates AQP expression in parental cells.**
824 To investigate whether PHB2 regulates AQP expression, PHB knockdown
825 experiments were performed. **A:** Relative PHB2 expression. **B:** Relative AQP3
826 expression. **C:** Relative AQP5 expression. **D:** Relative AQP8 expression. PHB2
827 knockdown led to upregulated AQP expression. **: $p < 0.01$ using Student's
828 *t*-test (vs. N.C.).
829
830 **Fig. 9. Schematic diagram of mitochondria-mediated ferroptosis by H_2O_2.**
831 H_2O_2 permeability is regulated by cell surface AQPs. Intracellular H_2O_2
832 becomes $^{\bullet}OH$ by the Fenton reaction. The peroxidized phospholipids induced by
833 $^{\bullet}OH$ in the plasma and mitochondrial membrane suggest the high probability of
834 ferroptosis. We propose that internal H_2O_2 levels also increase via NOX2, which
835 is bound to AQPs and produces H_2O_2 at the plasma membrane. In mitochondria,
836 oxidative phosphorylation produces $O_2^{\bullet -}$, which is converted to $^{\bullet}OH$. ρ^0 cells
837 could produce more $^{\bullet}OH$ than parental cells because of lacking mtDNA and
838 mitochondrial dysfunction, such as enhancement of mitochondrial membrane
839 permeability and PHB2 reduction. PHB2 may negatively regulates AQP
840 expression via ERα, and inhibits enhanced H_2O_2 permeability through the
841 plasma and mitochondrial membranes. In other words, mitochondrial
842 dysfunction, which is present in ρ^0 cells, enhance mitochondrial leak of Fe^{2+},

843 which further promotes mitochondrial and cytoplasmic Fenton reactions, leading
844 to ferroptosis via enhanced $^{\bullet}OH$ production and lipid peroxidation. Reduction of
845 GPx4 via Nrf2 would be caused by mitochondrial dysfunction and accelerate
846 plasma membrane lipid peroxidation. See the detail for discussion section.
847

848 **Table 1. Primer sequences used in this study**

849

Primer name	Primer sequence
AQP3-F	5'-TTTTTACAGCCCTTGCGGGCTGGG-3'
AQP3-R	5'-ATCATCAGCTGGTACACGAAGACACC-3'
AQP5-F	5’-ATGAACCCAGCCCGCTCTTTTGGC-3’
AQP5-R	5’-ACGCTCACTCAGGCTCAGGGAGTT-3’
AQP8-F	5'-AACCACTGGAACTTCCACTGGATCTACT-3'
AQP8-R	5'-ATCTCCAATGAAGCACCTAATGAGCAGTC-3'
PHB2-F	5’-AAGATGCTTGGAGAAGCACTGAGCAAGAA-3’
PHB2-R	5’-AGCACAAGGTTGTCAGCTGTGAGATAGATA-3’
β actin-F	5’-AGAGCTACGAGCTGCCTGAC-3’
β actin-R	5’-AGCACTGTGTTGGCGTACAG-3’

850

851

852

853 **Table 2. Effect of H_2O_2 treatment on cell viability after AQP knockdown**
854 **(Result of statistical analysis of Fig. 5 A and B)**
855

HeLa ρ^0	12.5 μM	25 μM	50 μM	100 μM	200μM
siAQP3	*	*	**	*	
siAQP5			*	**	
siAQP8	*	**	**	**	**

SAS ρ^0	12.5 μM	25 μM	50 μM	100 μM	200μM
siAQP3		**	**	**	**
siAQP5		**	**	**	**
siAQP8	**	*		**	**

856
857 *: $p < 0.05$, **: $p < 0.01$ by Scheffe's F test compared with negative control.
858
859

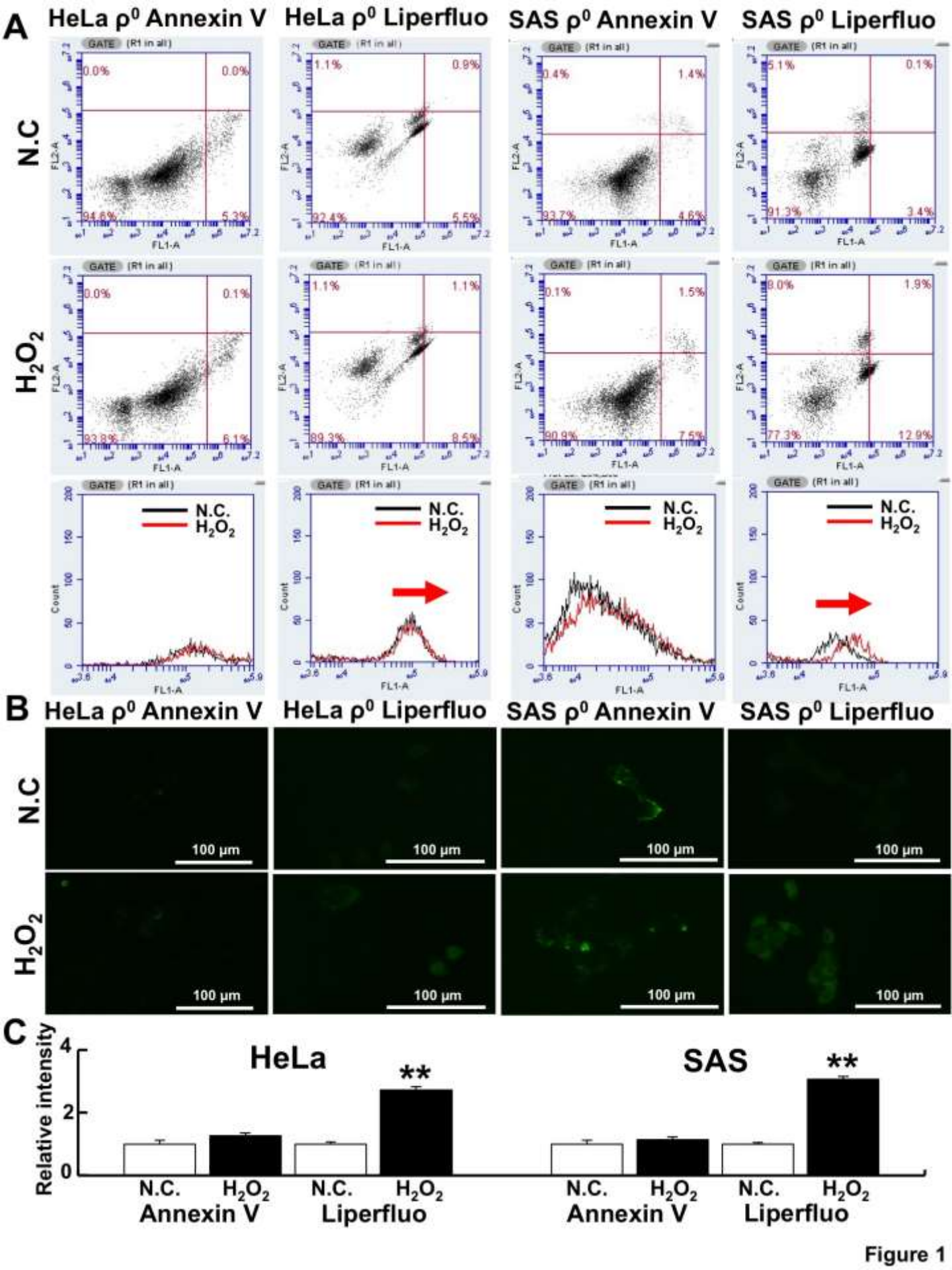
A
HeLa ρ0 Annexin V
HeLa ρ0 Liperfluo
SAS ρ0 Annexin V
SAS ρ0 Liperfluo
N.C
H2O2
GATE (R1 in all)
FL1-A
FL2-A
Count
N.C.
H2O2
B
100 μm
C
Relative intensity
HeLa
SAS
**
N.C.
H2O2
Annexin V
Liperfluo

Figure 1

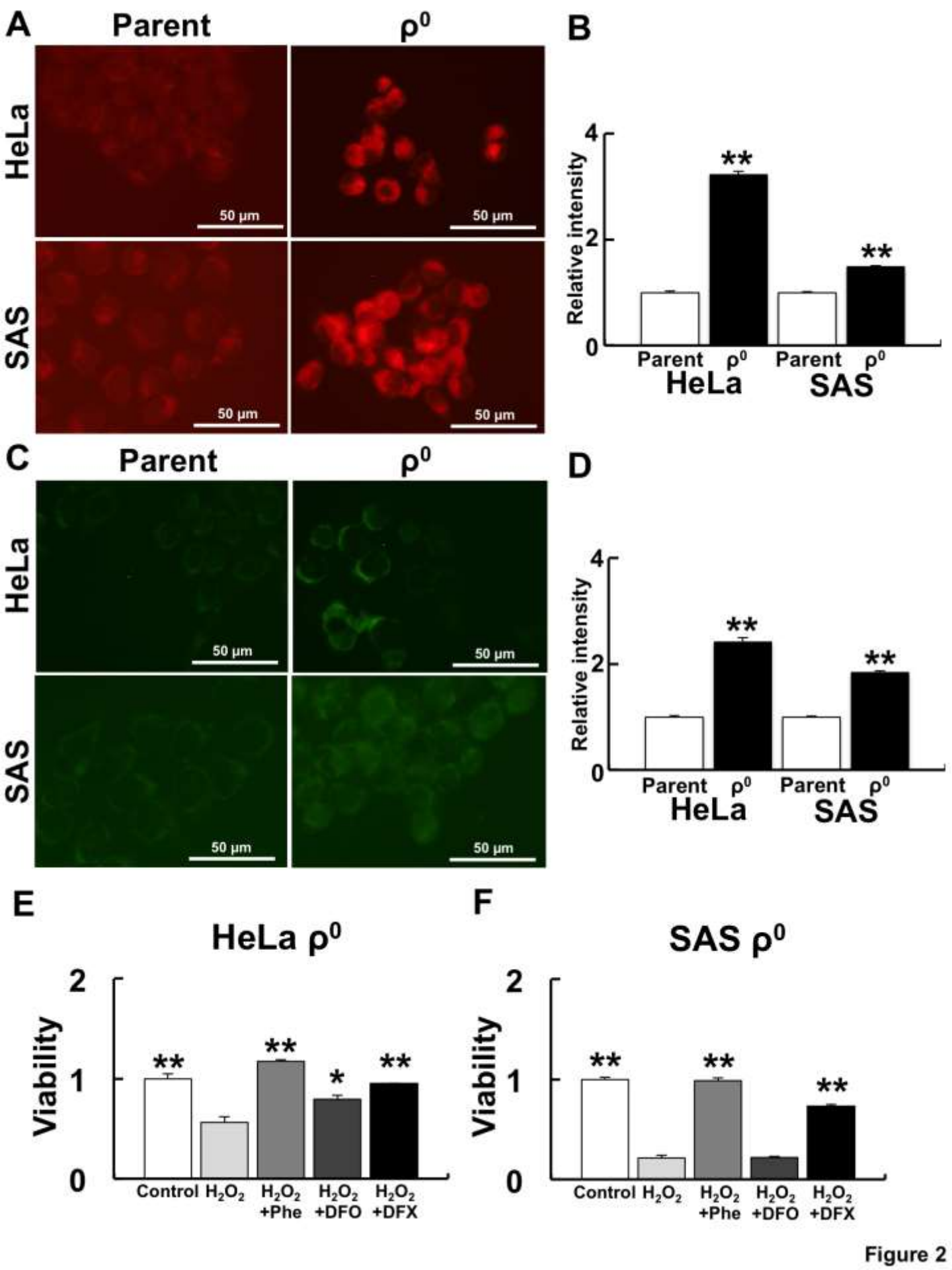
A
Parent
ρ0
HeLa
SAS
50 μm
B
Relative intensity
4
2
0
**
Parent
ρ0
HeLa
SAS
C
D
E
HeLa ρ0
Viability
Control
H2O2
H2O2 +Phe
H2O2 +DFO
H2O2 +DFX
*
F
SAS ρ0

Figure 2

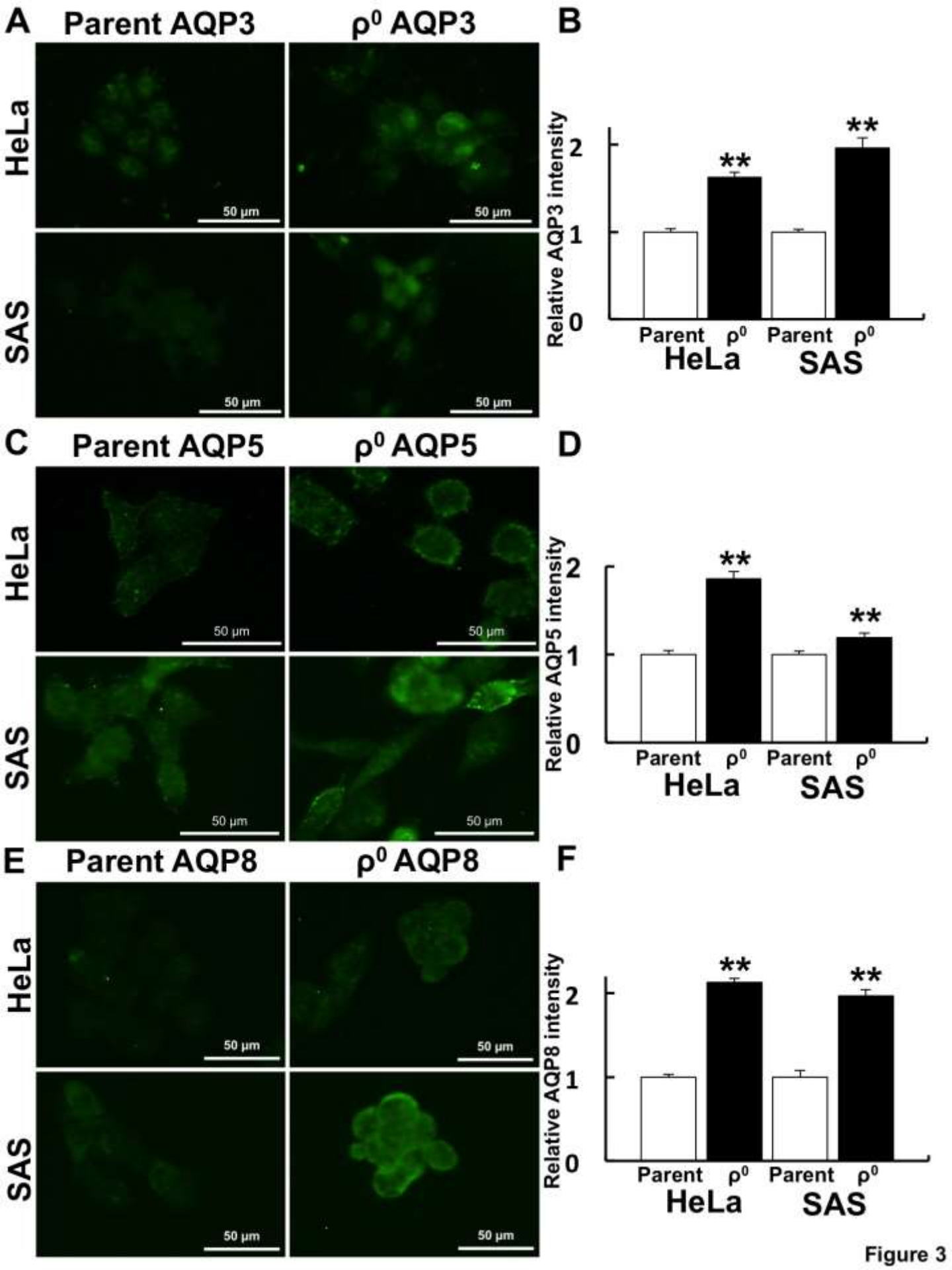
A
Parent AQP3
ρ0 AQP3
HeLa
SAS
50 μm
B
Relative AQP3 intensity
0
1
2
**
Parent
ρ0
HeLa
SAS
C
Parent AQP5
ρ0 AQP5
D
Relative AQP5 intensity
E
Parent AQP8
ρ0 AQP8
F
Relative AQP8 intensity

Figure 3

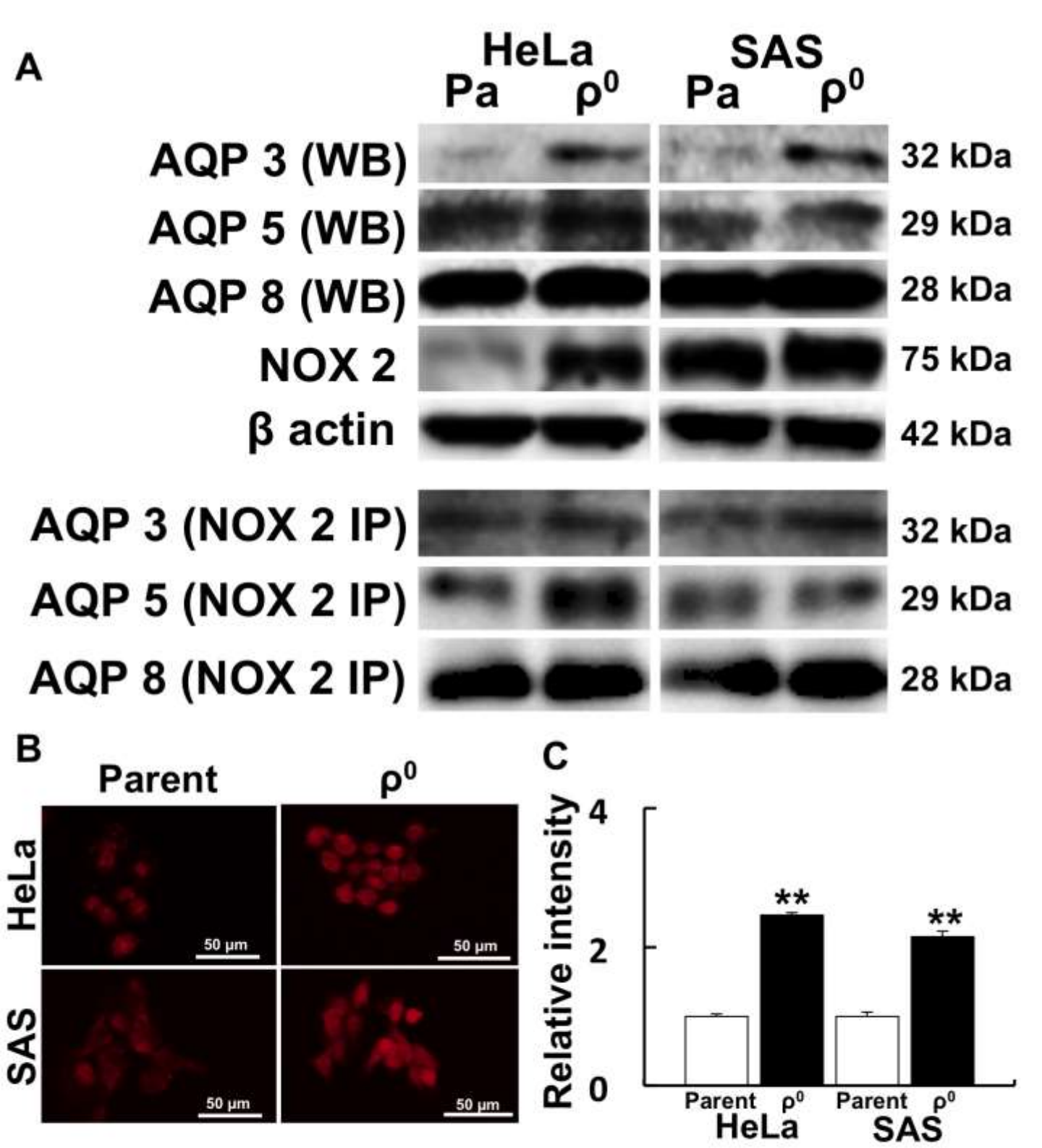
A
HeLa
SAS
Pa
ρ0
Pa
ρ0
AQP 3 (WB)
32 kDa
AQP 5 (WB)
29 kDa
AQP 8 (WB)
28 kDa
NOX 2
75 kDa
β actin
42 kDa
AQP 3 (NOX 2 IP)
32 kDa
AQP 5 (NOX 2 IP)
29 kDa
AQP 8 (NOX 2 IP)
28 kDa
B
Parent
ρ0
HeLa
SAS
50 μm
50 μm
50 μm
50 μm
C
Relative intensity
4
2
0
**
**
Parent
ρ0
Parent
ρ0
HeLa
SAS

Figure 4

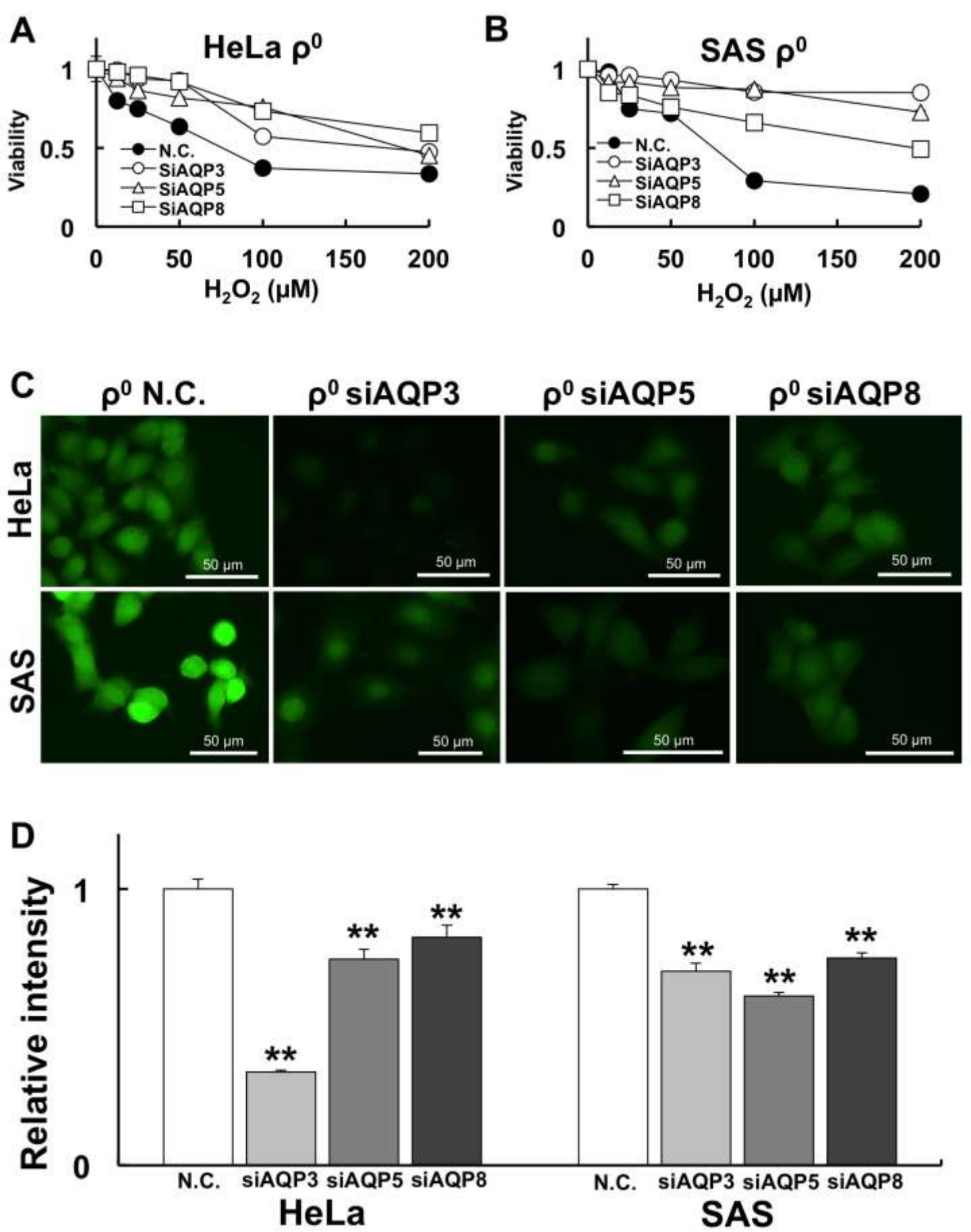
A
HeLa ρ0
Viability
1
0.5
0
N.C.
SiAQP3
SiAQP5
SiAQP8
0
50
100
150
200
H2O2 (μM)
B
SAS ρ0
Viability
1
0.5
0
N.C.
SiAQP3
SiAQP5
SiAQP8
0
50
100
150
200
H2O2 (μM)
C
ρ0 N.C.
ρ0 siAQP3
ρ0 siAQP5
ρ0 siAQP8
HeLa
SAS
50 μm
D
Relative intensity
1
0
**
N.C.
siAQP3
siAQP5
siAQP8
HeLa
SAS

Figure 5

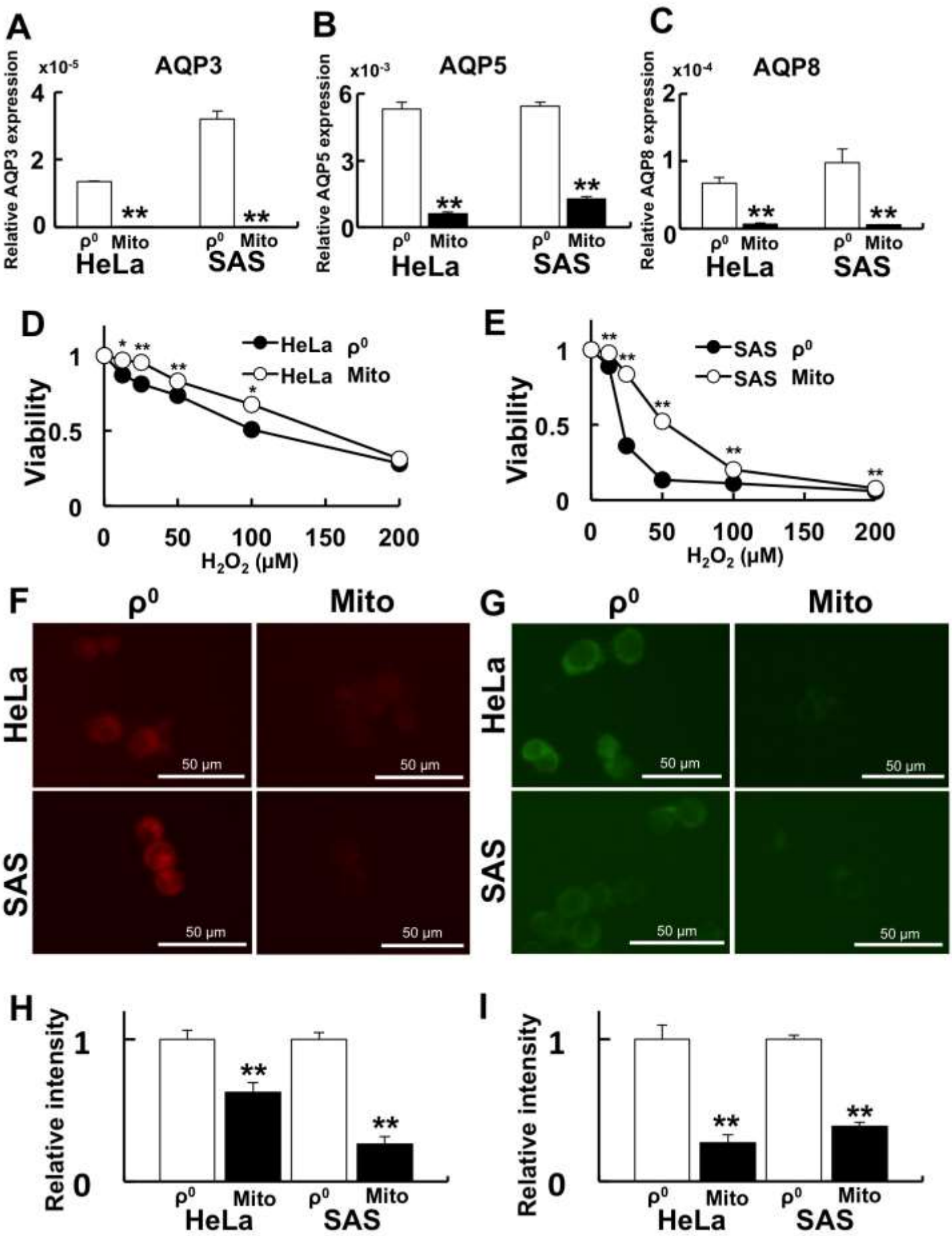
A
AQP3
x10-5
Relative AQP3 expression
4
2
0
**
**
ρ0 Mito
ρ0 Mito
HeLa
SAS
B
AQP5
x10-3
Relative AQP5 expression
6
3
0
**
**
ρ0 Mito
ρ0 Mito
HeLa
SAS
C
AQP8
x10-4
Relative AQP8 expression
2
1
0
**
**
ρ0 Mito
ρ0 Mito
HeLa
SAS
D
Viability
1
0.5
0
HeLa ρ0
HeLa Mito
0 50 100 150 200
H2O2 (μM)
E
Viability
1
0.5
0
SAS ρ0
SAS Mito
0 50 100 150 200
H2O2 (μM)
F
ρ0
Mito
HeLa
SAS
50 μm
G
ρ0
Mito
HeLa
SAS
50 μm
H
Relative intensity
1
0
**
**
ρ0 Mito
ρ0 Mito
HeLa
SAS
I
Relative intensity
1
0
**
**
ρ0 Mito
ρ0 Mito
HeLa
SAS

Figure 6

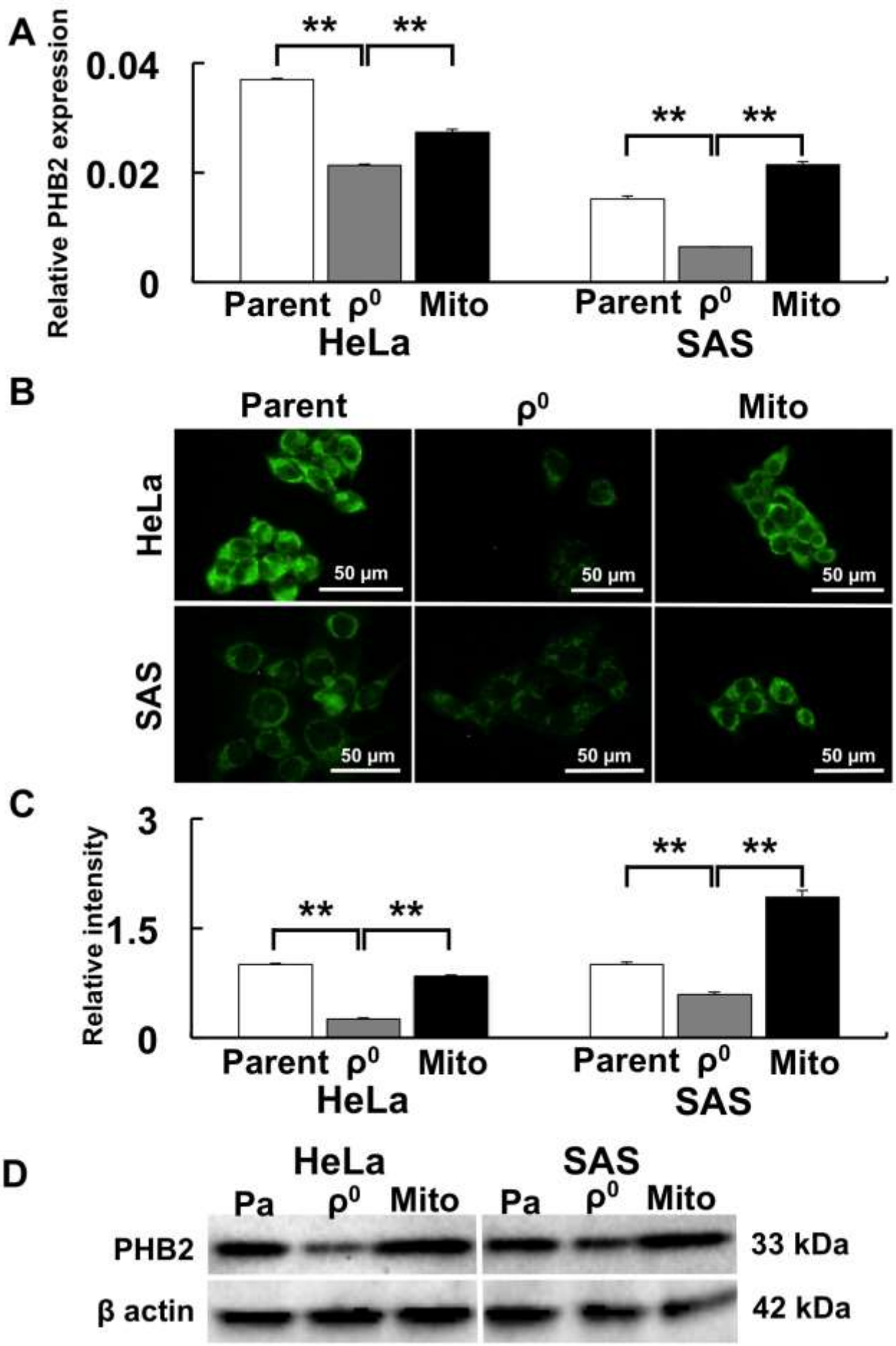
A
Relative PHB2 expression
0.04
0.02
0
**
**
**
**
Parent
ρ0
Mito
HeLa
Parent
ρ0
Mito
SAS
B
Parent
ρ0
Mito
HeLa
SAS
50 μm
C
Relative intensity
3
1.5
0
**
**
**
**
Parent
ρ0
Mito
HeLa
Parent
ρ0
Mito
SAS
D
HeLa
SAS
Pa
ρ0
Mito
Pa
ρ0
Mito
PHB2
β actin
33 kDa
42 kDa

Figure 7

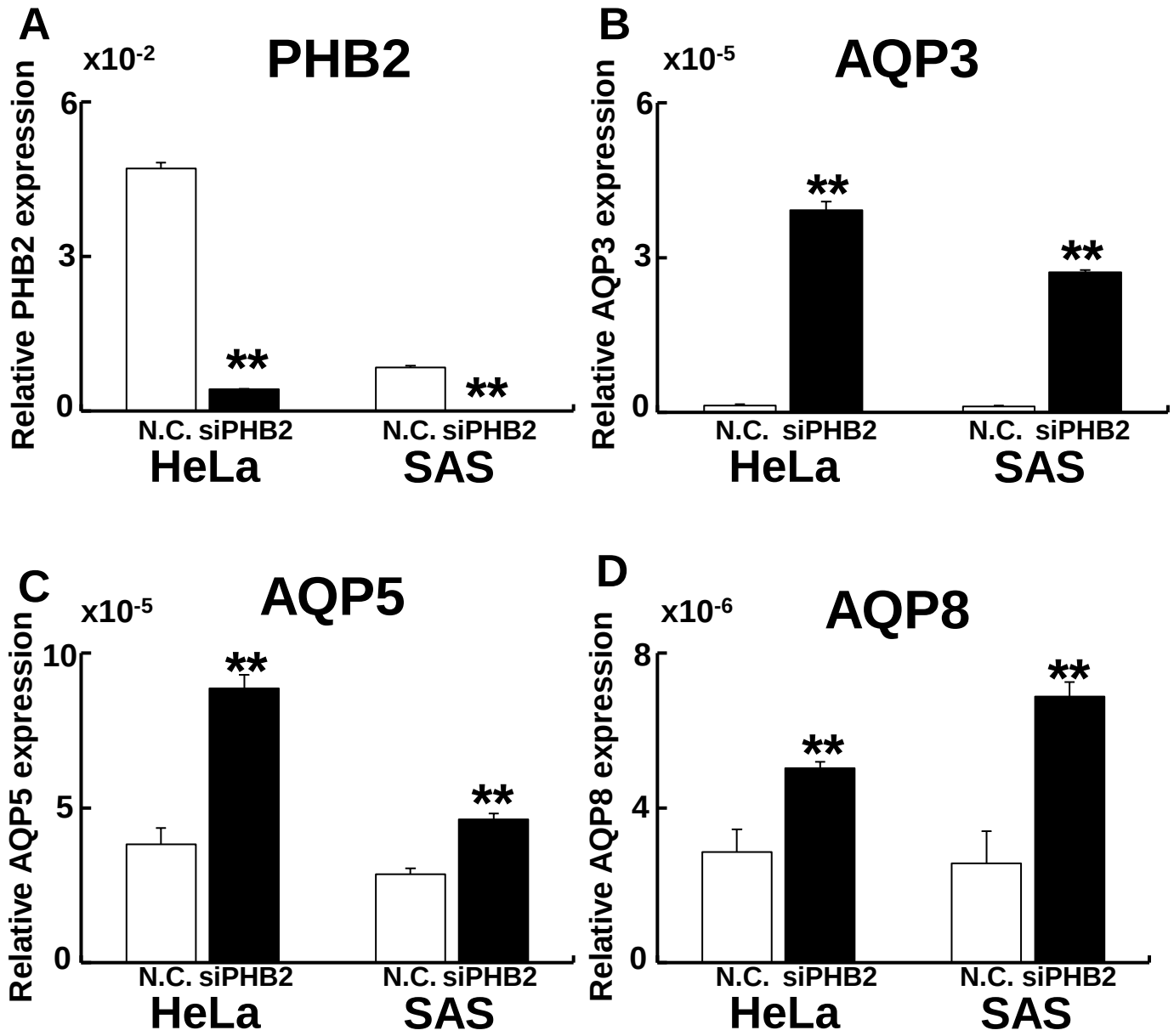
A
PHB2
x10-2
Relative PHB2 expression
6
3
0
**
**
N.C. siPHB2
N.C. siPHB2
HeLa
SAS
B
AQP3
x10-5
Relative AQP3 expression
6
3
0
**
**
N.C. siPHB2
N.C. siPHB2
HeLa
SAS
C
AQP5
x10-5
Relative AQP5 expression
10
5
0
**
**
N.C. siPHB2
N.C. siPHB2
HeLa
SAS
D
AQP8
x10-6
Relative AQP8 expression
8
4
0
**
**
N.C. siPHB2
N.C. siPHB2
HeLa
SAS

Figure 8

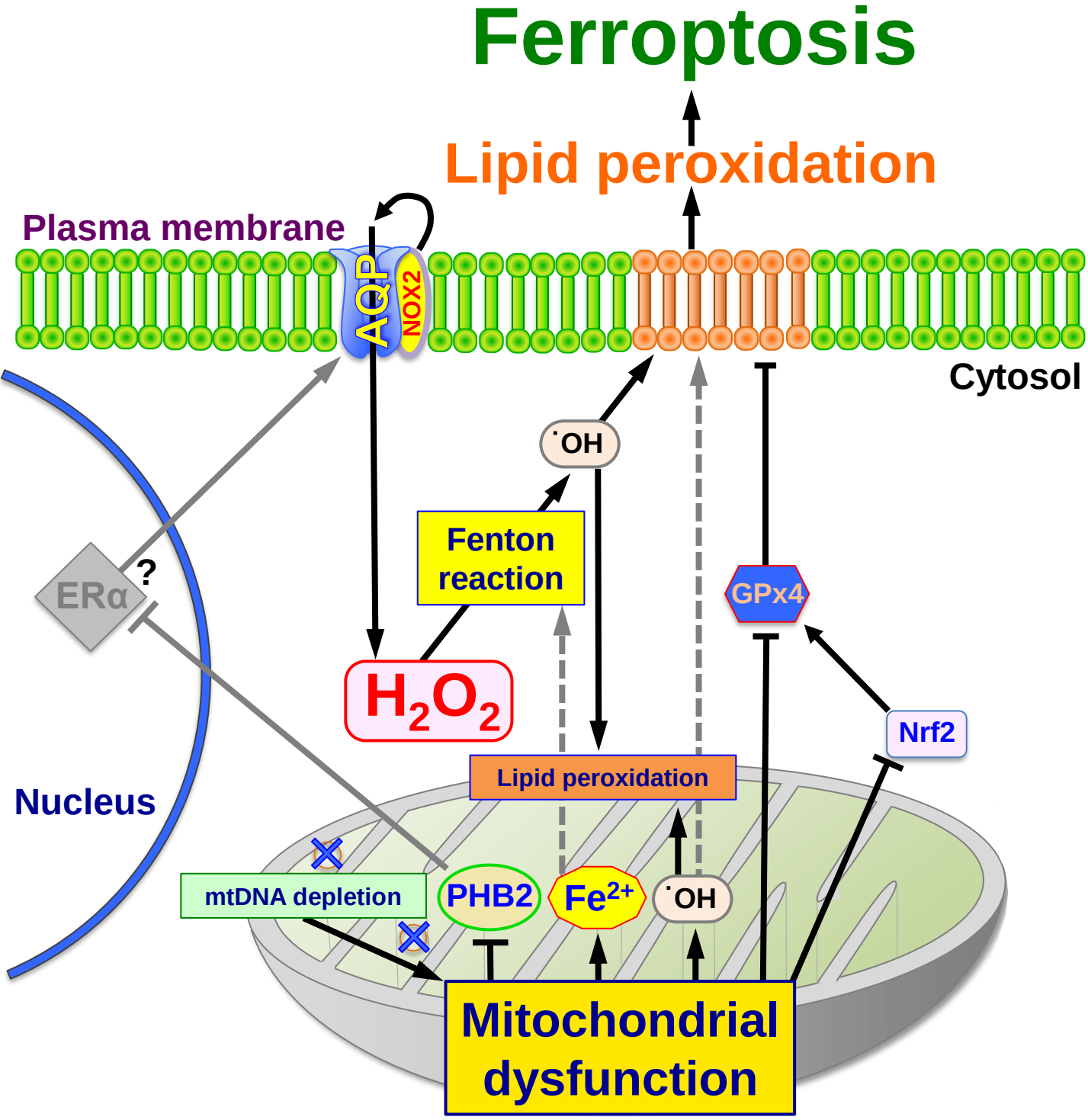
Ferroptosis
Lipid peroxidation
Plasma membrane
AQP
NOX2
Cytosol
˙OH
Fenton reaction
ERα
?
GPx4
H_2O_2
Nrf2
Lipid peroxidation
Nucleus
mtDNA depletion
PHB2
Fe^{2+}
˙OH
Mitochondrial dysfunction

Figure 9

Table 1. Primer sequences used in this study

Primer name	Primer sequence
AQP3-F	5'-TTTTTACAGCCCTTGCGGGCTGGG-3'
AQP3-R	5'-ATCATCAGCTGGTACACGAAGACACC-3'
AQP5-F	5’-ATGAACCCAGCCCGCTCTTTTGGC-3’
AQP5-R	5’-ACGCTCACTCAGGCTCAGGGAGTT-3’
AQP8-F	5'-AACCACTGGAACTTCCACTGGATCTACT-3'
AQP8-R	5'-ATCTCCAATGAAGCACCTAATGAGCAGTC-3'
PHB2-F	5’-AAGATGCTTGGAGAAGCACTGAGCAAGAA-3’
PHB2-R	5’-AGCACAAGGTTGTCAGCTGTGAGATAGATA-3’
β actin-F	5’-AGAGCTACGAGCTGCCTGAC-3’
β actin-R	5’-AGCACTGTGTTGGCGTACAG-3’

Table 2. Effect of H_2O_2 treatment on cell viability after AQP knockdown

HeLa ρ^0	12.5 μM	25 μM	50 μM	100 μM	200μM
siAQP3	*	*	**	*	
siAQP5			*	**	
siAQP8	*	**	**	**	**

SAS ρ^0	12.5 μM	25 μM	50 μM	100 μM	200μM
siAQP3		**	**	**	**
siAQP5		**	**	**	**
siAQP8	**	*		**	**

*: $p < 0.05$, **: $p < 0.01$ by Scheffe's F test compared with N.C.

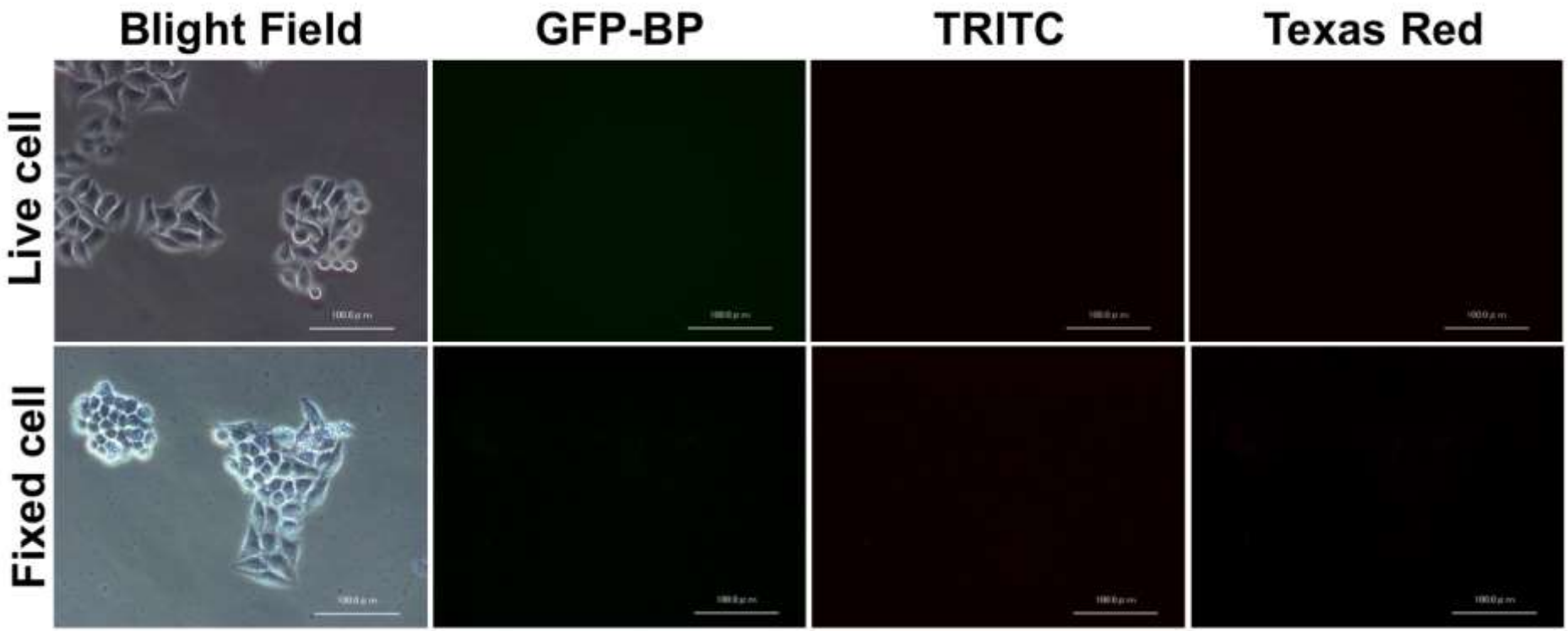

Figure S1

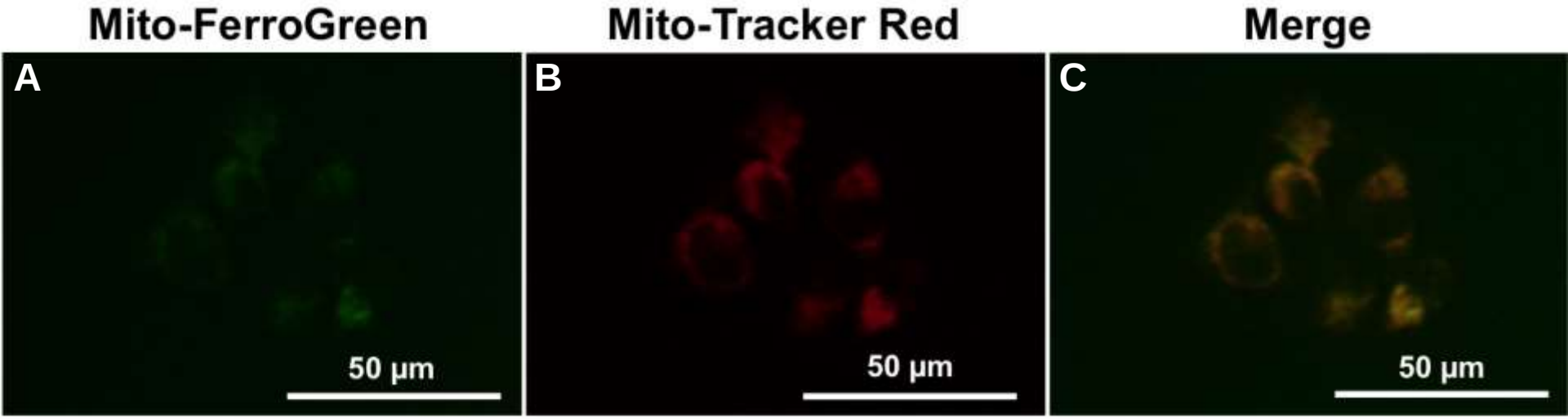

Figure S2

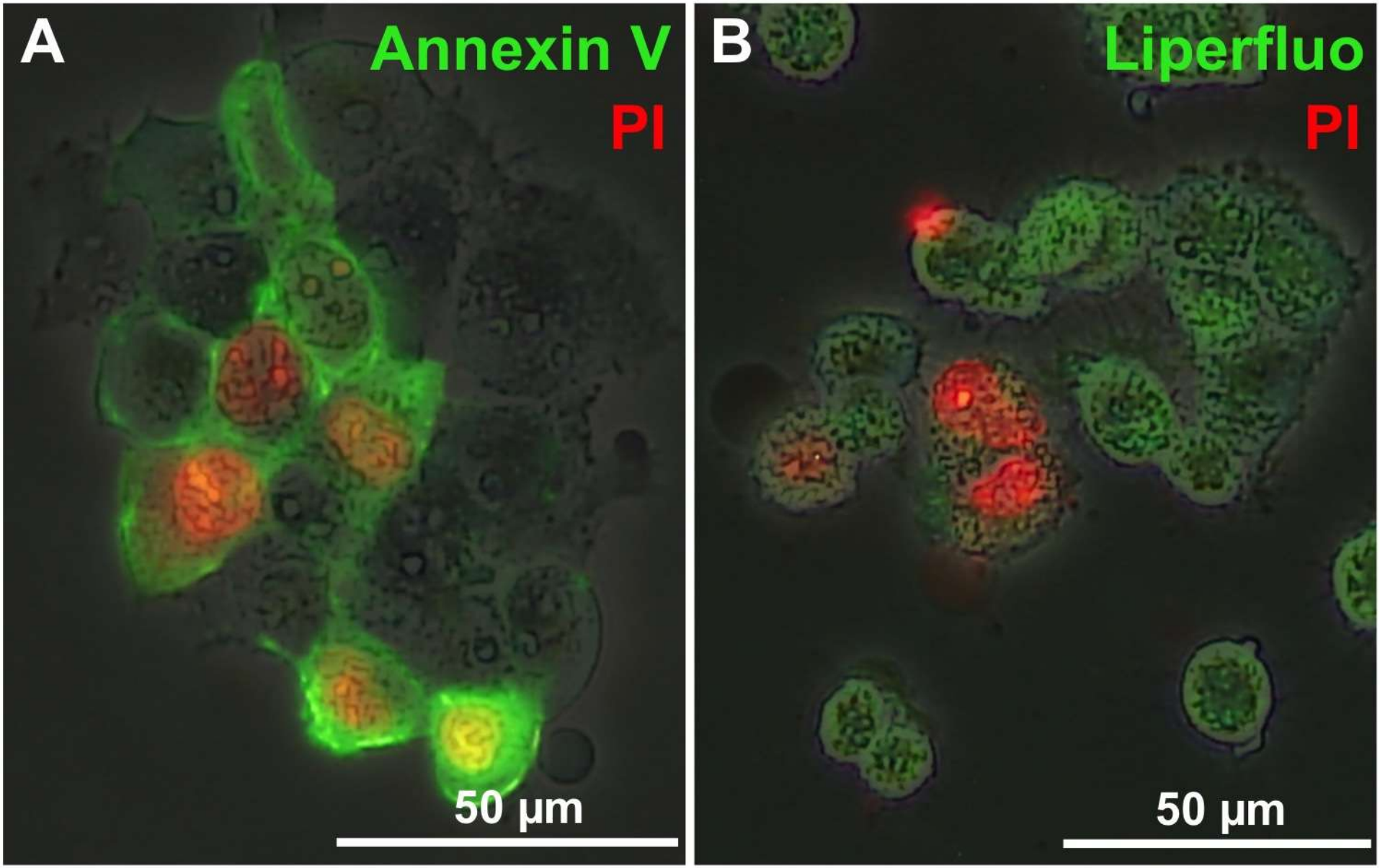

Figure S3

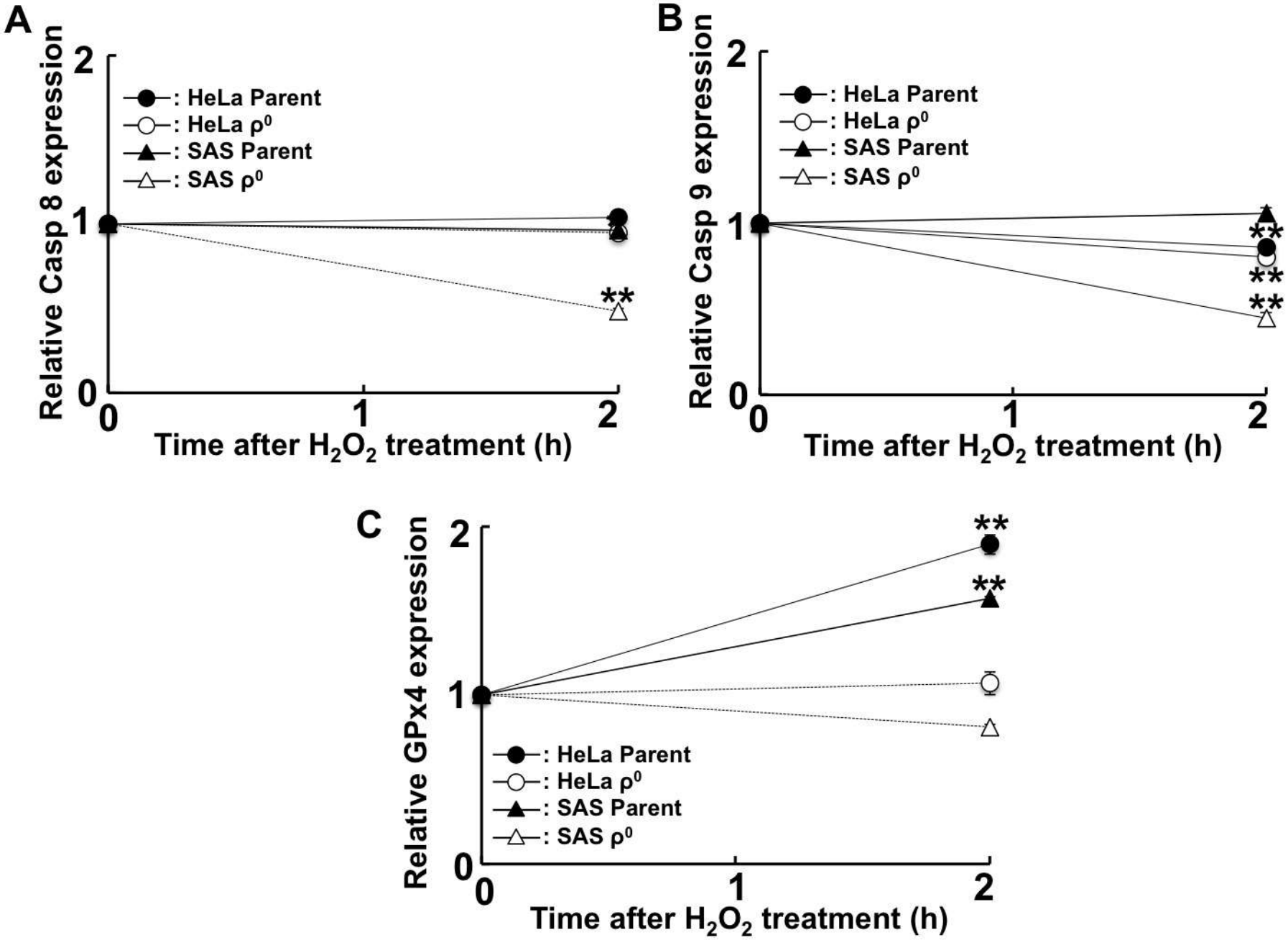
A
Relative Casp 8 expression
2
1
0
: HeLa Parent
: HeLa ρ0
: SAS Parent
: SAS ρ0
**
0
1
2
Time after H2O2 treatment (h)
B
Relative Casp 9 expression
2
1
0
: HeLa Parent
: HeLa ρ0
: SAS Parent
: SAS ρ0
**
**
**
0
1
2
Time after H2O2 treatment (h)
C
Relative GPx4 expression
2
1
0
**
**
: HeLa Parent
: HeLa ρ0
: SAS Parent
: SAS ρ0
0
1
2
Time after H2O2 treatment (h)

Figure S4

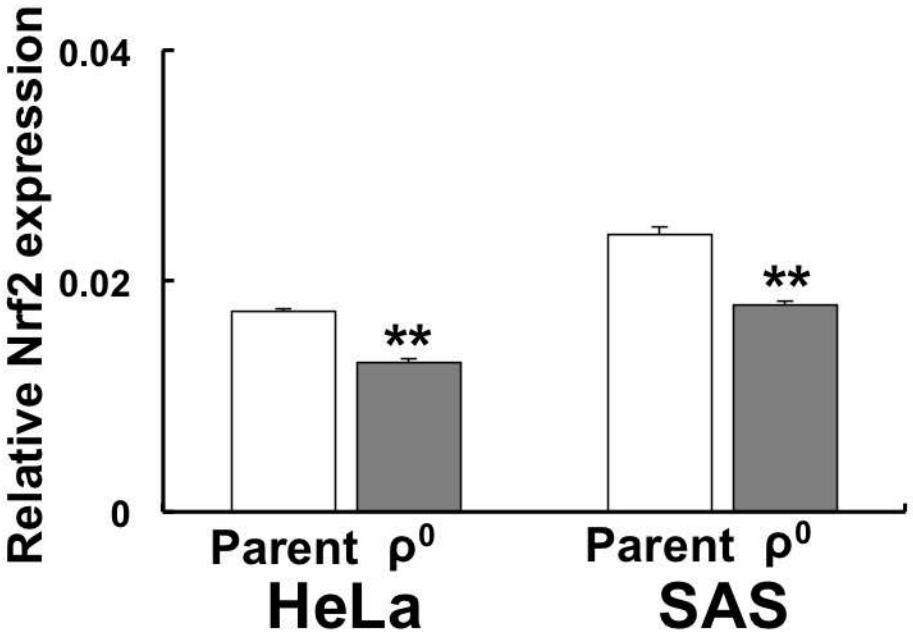
Relative Nrf2 expression
0.04
0.02
0
**
**
Parent
ρ0
Parent
ρ0
HeLa
SAS

Figure S5

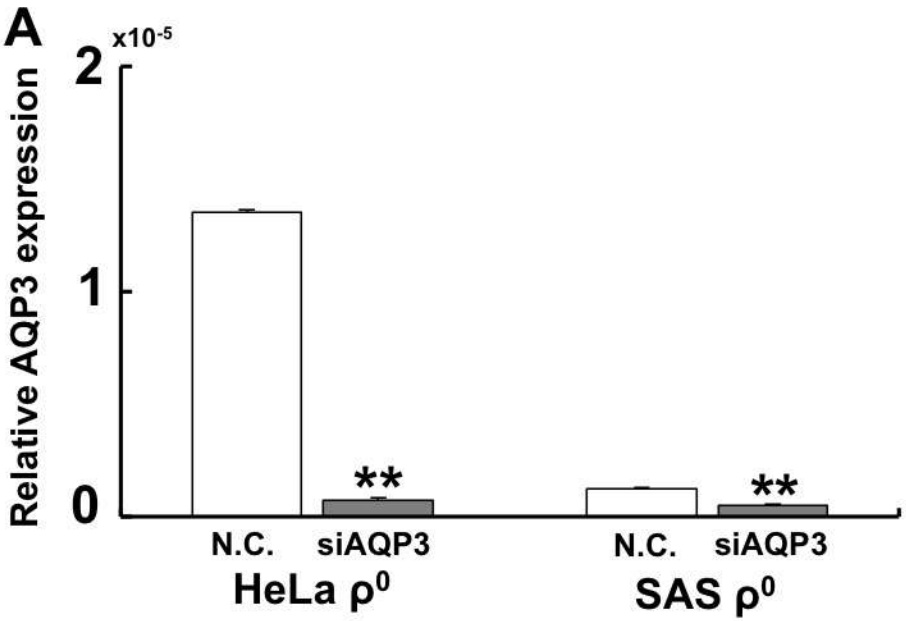
A
x10-5
2
1
0
Relative AQP3 expression
**
**
N.C.
siAQP3
N.C.
siAQP3
HeLa ρ0
SAS ρ0

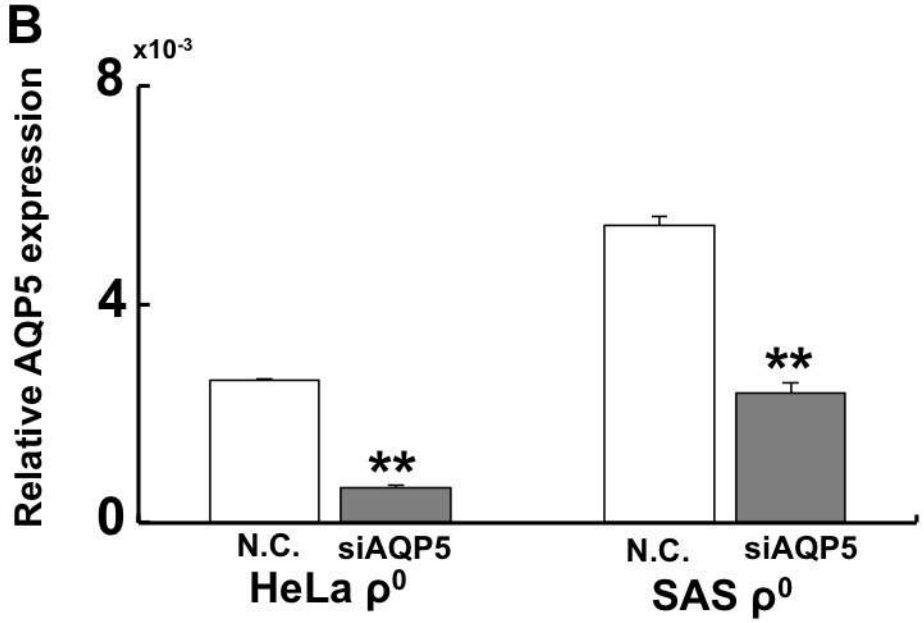
B
x10-3
8
4
0
Relative AQP5 expression
**
**
N.C.
siAQP5
N.C.
siAQP5
HeLa ρ0
SAS ρ0

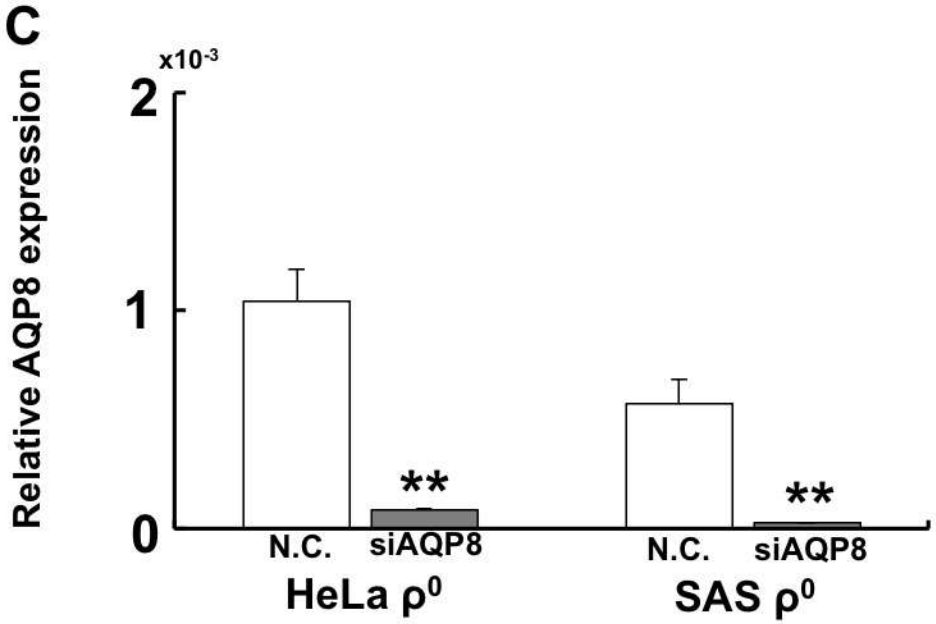
C
x10-3
2
1
0
Relative AQP8 expression
**
**
N.C.
siAQP8
N.C.
siAQP8
HeLa ρ0
SAS ρ0

Figure S6

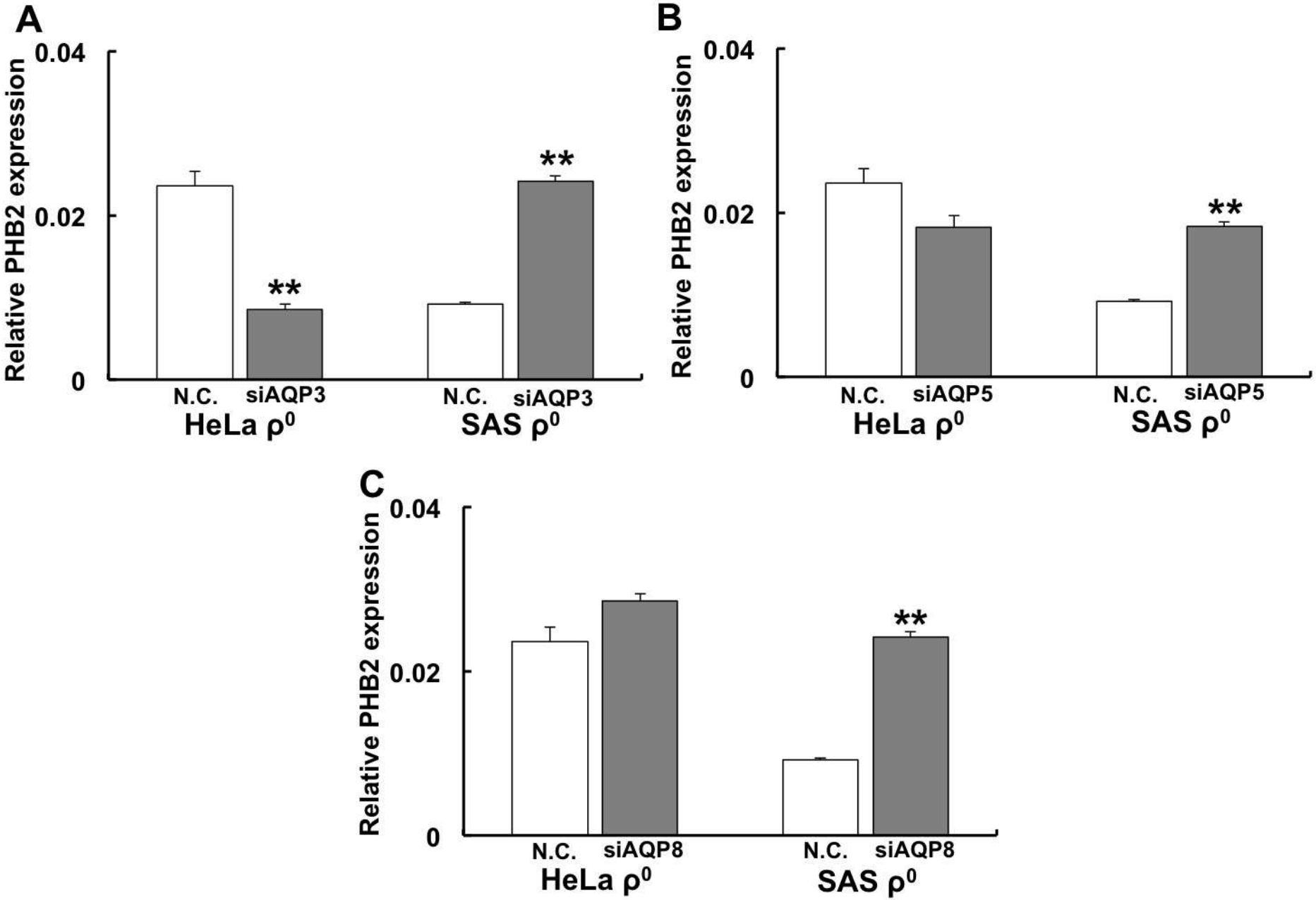
A
Relative PHB2 expression
0.04
0.02
0
**
**
N.C.
siAQP3
N.C.
siAQP3
HeLa ρ0
SAS ρ0
B
Relative PHB2 expression
0.04
0.02
0
**
N.C.
siAQP5
N.C.
siAQP5
HeLa ρ0
SAS ρ0
C
Relative PHB2 expression
0.04
0.02
0
**
N.C.
siAQP8
N.C.
siAQP8
HeLa ρ0
SAS ρ0

Figure S7

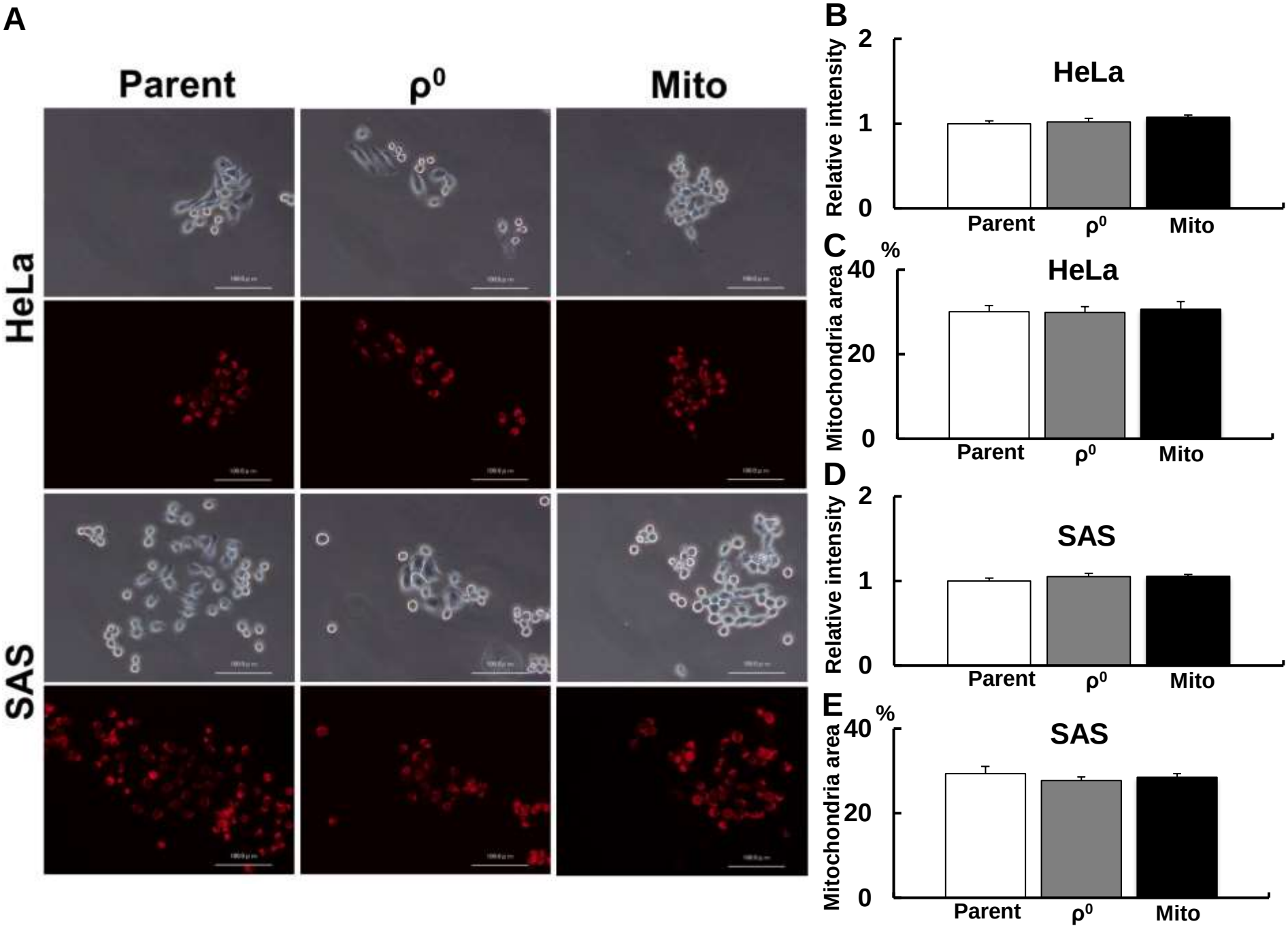
A
Parent
ρ0
Mito
HeLa
SAS
B
HeLa
Relative intensity
2
1
0
Parent
ρ0
Mito
C
HeLa
Mitochondria area
%
40
20
0
Parent
ρ0
Mito
D
SAS
Relative intensity
2
1
0
Parent
ρ0
Mito
E
SAS
Mitochondria area
%
40
20
0
Parent
ρ0
Mito

Figure S8

Table S1 Primer sequences used in this study for supplemental data

Primer name	Primer sequence
CASP8-F	5'-AGAGCGATGTCCTCGAGGCGATGATATT-3'
CASP8-R	5'-AAGTAGGCTGAGGCATCTGTTTCCCCAT-3'
CASP9-F	5’-CAAGAGTGGCTCCTGGTACGTTGAGA-3’
CASP9-R	5’-CTGTTTATAAATCCCTTTCACCGAAACAGC-3’
GPx4-F	5'-GAGCCAGGGAGTAACGAAGAGATCAAA -3'
GPx4-R	5'-TCACGCAGATCTTGCTGAACATATCGAATT-3'
Nrf2-F	5'-TCAGCCAGCCCAGCACATCC-3'
Nrf2-R	5'-TCTGCGCCAAAAGCTGCATGC-3'
Nfkb-F	5'-CAATGCCCTTTTCGACTACG-3'
Nfkb-R	5'-GGTGGATGATTGCTAAGTGTAAGA-3'
β actin-F	5’-AGAGCTACGAGCTGCCTGAC-3’
β actin-R	5’-AGCACTGTGTTGGCGTACAG-3’

Fig S1. Autofluorescence analysis using a BZ-8000 fluorescence microscope.

To show the absence of autofluorescence, images were taken with the same filters and exposure times without probes. Upper row: Live cells. Lower row: Fixed cells. From the left, bright field, GFP-BP, Texas Red, and TRITC images. No autofluorescence was detected under the conditions of this experiment. Bar: 100 µm.

Fig S2. Merged image of Mito-Ferrogreen and MitoTracker.

Cells were stained with 50 nM Mito-Tracker red CMXRos and 5 µM Mito-FerroGreen in HBSS without serum for 30 min at 37 ºC. Then, Mito-Tracker red CMXRos and Mito-FerroGreen were removed by washing with HBSS. Cells were imaged using a BZ-8000 fluorescence microscope with GFP-BP and Texas Red filters. A: Mito-FerroGreen. B: Mito-Tracker red CMXRos. C: Merged image. Mito-FerroGreen and Mito-Tracker red CMXRos were detected as a yellow signal because the staining location was the same. Bar: 50 µm.

Fig S3. Typical Annexin V (apoptosis) or Liperfluo (ferroptosis) images.

Cells were stained with Annexin V or Liperfluo with PI after H_2O_2 treatment, as described in the Materials and methods. A. Detection of apoptosis by Annexin V in SAS parental cells. B. Detection of ferroptosis by Liperfluo in HeLa ρ^0 cells. Early apoptosis/ferroptosis (green only) and late apoptosis/ferroptosis (green and red staining) were observed. Bar: 50 µm.

Fig S4. Gene expression of Caspase 8, 9, and GPx4 in ρ^0 cells after H_2O_2 treatment.

Gene expression of the apoptosis markers (Caspase 8 and Caspase 9) and the anti-ferroptosis marker GPx4 were examined after cells were treated with 75 µM (for HeLa cells) or 50 µM (for SAS cells) H_2O_2 for 2 h. After qPCR, the relative gene expression ratios compared with 0 h (No H_2O_2 treatment) were calculated. A: Relative Caspase 8 expression. B: Relative Caspase 9 expression. C: Relative GPx4 expression. Expression of apoptosis markers was not upregulated, but rather downregulated in ρ^0 cells. In contrast, GPx4 gene expression, which protects against ferroptosis, was not activated in ρ^0 cells.

The lack of elevated GPx4 expression indicates that ρ^0 cells are not protected from ferroptosis after H_2O_2 treatment. **: $p < 0.01$ using Student's *t*-test (vs negative control). Primer sequences are listed in Table S1.

Fig S5. Nrf2 gene expression in ρ^0 cells.

Because Nrf2 has been reported to regulate GPx4, Nrf2 gene expression was examined. Nrf2 expression was downregulated in ρ^0 cells. N.C.: Negative control. **: $p < 0.01$ using Student's *t*-test (vs parent). Primer sequences are listed in Table S1..

Fig S6. AQP gene expression in ρ^0 cells after siAQP treatment.

To confirm siAQP transfection, AQP expression in ρ^0 cells after siAQP treatment was examined. Specific gene knockdown was observed in all siRNA treatments, indicating that the siRNA treatment worked well. **: $p < 0.01$ using Student's *t*-test (vs N.C.).

Fig S7. PHB2 gene expression in ρ^0 cells after siAQP treatment.

To investigate whether the PHB2 gene was under the control of AQPs, PHB2 gene expression was examined after siAQP treatment. The PHB2 gene is not regulated by AQPs. **: $p < 0.01$ using Student's *t*-test (vs N.C.).

Fig S8. Mito-Tracker staining and measurement of mitochondrial area.

Cells were stained with 50 nM Mito-Tracker red CMXRos in HBSS without serum for 30 min at 37 ° C. Mito-Tracker was removed by washing with HBSS and observed using a BZ-8000 fluorescence microscope with a Texas Red filter. The cellular area occupied by mitochondria was determined by calculating the ratio of the area of the entire cell to the area stained with Mito-Tracker red CMXRos. Cells with similar shapes were selected in each condition, and more than 10 cells from three independent dishes under each condition were analyzed. A: Blight field and fluorescent images of parent, ρ^0 and Mito cells. B: Relative intensity of Mito-Tracker red CMXROS in HeLa cells. C: Measurement of mitochondrial area in HeLa cells. D: Relative intensity of Mito-Tracker red CMXRos in SAS cells. E: Measurement of mitochondrial area in SAS cells. There was no significant difference among parent, ρ^0, and Mito cells in fluorescence intensity or mitochondrial area. Bar: 100 µm.

Table S1 Primer sequences used in this study for supplemental data

The PCR conditions were the same as described in the Materials and methods.